

**POLITECNICO DI TORINO**

**Master's degree in Mechatronic Engineering**

**FINAL THESIS PROJECT**

**FOOD QUALITY MONITORING USING**  
**HYPERSPECTRAL DATA**



*Supervised by:*

***Prof. Tiziano Bianchi***  
***Prof. Rafic Younes***

*Student:*

***Nabih Abdallah***

2019/2020

## **ACKNOWLEDGEMENTS**

I would like to express my great appreciation to Prof. Tiziano Bianchi and Prof. Rafic Younes, for their valuable and constructive suggestions, their continuous support and guidance, for their patience, motivation and immense knowledge during the planning and development of this research work. their willingness to give their time so generously has been very much appreciated.

Also, I would like to thank the National Council for Scientific Research (*CNRS*) for allowing me to use their equipments. In addition, I would like to thank Dr. Mohammad Awad for his help in operating the spectroradiometer used in the acquisition of the meat hyperspectral data.

Furthermore, I would also like to acknowledge with much appreciation the crucial role of Dr. Ihab Makki, whose contribution throughout this project, especially his knowledge in Matlab, has been very helpful in the successful completion of this research.

Finally, I would like to thank both the Politecnico Di Torino and the Lebanese University, the former for allowing me the chance to do my thesis abroad, and the latter for its support in making its laboratory and equipments available for researchers.

## **ABSTRACT**

Hyperspectral imaging (HSI) technology is an innovative, nondestructive method that found its way to various fields including the quality evaluation of different food products. This thesis tackled the application of hyperspectral imaging in food monitoring, more specifically detecting meat degradation through the analysis of their hyperspectral data. Building on existing work on hyperspectral imaging, it asks: Could spoiled meat be detected based on its hyperspectral signature? Can this technique predict how fresh meat is, i.e. at which stage of deterioration it currently resides? In this context, hyperspectral image processing involves the use of computer programs to extract, store and process information from certain bands in the electromagnetic spectrum and utilize this information to differentiate between materials and detect the presence of certain materials in different objects.

Based on a review of the literature concerning hyperspectral imaging and the different methods used to detect meat spoilage, this research studied the hyperspectral signals of several fresh and spoiled meat. Then, many cross-correlation values were computed, and their results were complemented by analyzing the reflectance of meat samples that were measured by a spectroradiometer. The results showed interesting findings concerning the meat signatures and the different amount of light they reflect in different bandwidths. However, they could not establish a solid relationship between meat deterioration level and their hyperspectral data. Finally, some propositions have been presented into how hyperspectral imaging can best be applied to the food industry and the different ways future research could obtain more conclusive results.

## TABLE OF CONTENTS

<b>LIST OF FIGURES .....</b>	<b>VI</b>
<b>LIST OF TABLES .....</b>	<b>VIII</b>
<b>CHAPTER 1: INTRODUCTION.....</b>	<b>1</b>
<b>CHAPTER 2: LITERATURE REVIEW .....</b>	<b>3</b>
2.1    INTRODUCTION.....	3
2.2    DIGITAL IMAGES .....	3
2.2.1 <i>Grayscale Imaging</i> .....	4
2.2.2 <i>RGB Imaging</i> .....	5
2.2.3 <i>CMYK Imaging</i> .....	7
2.3    COLOR BIT DEPTH.....	8
2.4    ELECTROMAGNETIC SPECTRUM .....	10
2.5    METHODS OF DETECTING MEAT SPOILAGE.....	12
2.6    HYPERSPECTRAL IMAGING.....	18
2.6.1 <i>Hyperspectral Imaging Definition</i> .....	18
2.6.2 <i>Hypercube</i> .....	20
2.6.3 <i>Hyperspectral Imaging Applications</i> .....	23
2.6.4 <i>Benefits of Hyperspectral Imaging in Food Application</i> .....	27
2.7    CONCLUSION.....	28
<b>CHAPTER 3: STATE OF THE ART: PAPERS AND PAST RESEARCH....</b>	<b>29</b>
3.1    INTRODUCTION.....	29
3.2    PAST RESEARCH.....	29
3.2.1 <i>Hyperspectral Imaging for Nondestructive Determination of Some Quality Attributes for Strawberry</i> .....	29
3.2.2 <i>Line-Scan Hyperspectral Imaging Techniques for Food Safety and Quality Applications</i> .....	30
3.2.3 <i>Advanced Applications of Hyperspectral Imaging Technology for Food Quality and Safety Analysis and Assessment</i> .....	31
3.2.4 <i>Hyperspectral Imaging for Assessing Quality and Safety of Meat</i> .....	31
3.2.5 <i>Meat Quality Evaluation by Hyperspectral Imaging Technique</i> .....	32
3.2.6 <i>Evaluation of Near-Infrared Hyperspectral Imaging for Detection of Peanut and Walnut Powders in Whole Wheat Flour</i> .....	32
3.3    CONCLUSION.....	33
<b>CHAPTER 4: EXPERIMENTAL PROCEDURE &amp; RESULTS.....</b>	<b>34</b>
4.1    INTRODUCTION.....	34
4.2    HYPERSPECTRAL IMAGING DATA COLLECTION .....	34
4.2.1 <i>Material Selection &amp; Sampling</i> .....	34

4.2.2	<i>Meat Preparation</i> .....	35
4.2.3	<i>Measurement Devices</i> .....	36
4.2.4	<i>Hyperspectral Data Measurement</i> .....	39
4.3	RESULTS.....	40
4.3.1	<i>Reflectance Graphs</i> .....	40
4.3.2	<i>Cross-Correlations</i> .....	48
4.4	CONCLUSION .....	51
<b>CHAPTER 5: CONCLUSION.....</b>		<b>52</b>
<b>REFERENCES.....</b>		<b>54</b>

## LIST OF FIGURES

Figure 1: An example of a simplified (1-bit) grayscale digital image .....	4
Figure 2: An example of a grayscale image.....	5
Figure 3: An example of a digital image by three color matrices.....	7
Figure 4: The number of bits effect on color depth gradations.....	9
Figure 5: The electromagnetic spectrum.....	10
Figure 6: Visible light composition of the electromagnetic spectrum. ....	11
Figure 7: A schematic detailing the hypoxanthine detection process.....	14
Figure 8: The structure of a biosensor. ....	15
Figure 9: A schematic showing the basic elements of a biosensor.....	16
Figure 10: The device composed of modified carbon nanotubes. ....	17
Figure 11: A schematic of the operating principle of the optical sensor. ....	18
Figure 12: Differences in number of bands of the different type of imaging. ....	19
Figure 13: The hyperspectral image processing workflow typical steps.....	20
Figure 14: An example of a hypercube.....	21
Figure 15: An example of hyperspectral signal signature of Soil.....	21
Figure 16: An example of hyperspectral signal signature of Rock.....	22
Figure 17: An example of hyperspectral signal signature of Water. ....	22
Figure 18: An example of hyperspectral signal signature of Vegetation.....	23
Figure 19: A simple schematic of the satellite remote sensing process.....	24
Figure 20: The main difference between active and passive remote sensing. ....	24
Figure 21: The arrangement of meat samples during the meat preparation phase. ....	36
Figure 22: FieldSpec 4 HI-RES spectroradiometer. ....	37

Figure 23: ASD Illuminator Reflectance Lamp.....	38
Figure 24: Reflectance of meat at time equal to 1 hour.....	40
Figure 25: Reflectance of meat at time equal to 2 hours.....	41
Figure 26: Reflectance of meat at time equal to 4 hours.....	41
Figure 27: Reflectance of meat at time equal to 12 hours.....	42
Figure 28: Reflectance of meat at time equal to 16 hours.....	42
Figure 29: Reflectance of meat at time equal to 20 hours.....	43
Figure 30: Reflectance of meat at time equal to 24 hours.....	43
Figure 31: Reflectance of meat at time equal to 28 hours.....	44
Figure 32: Reflectance of meat at time equal to 36 hours.....	44
Figure 33: Reflectance of meat at time equal to 40 hours.....	45
Figure 34: Reflectance of meat at time equal to 44 hours.....	45
Figure 35: Reflectance of meat at time equal to 48 hours.....	46
Figure 36: Reflectance of fresh meat.....	46
Figure 37: Reflectance of different meat batches.....	47

## **LIST OF TABLES**

Table 1: FieldSpec 4 Hi-Res spectroradiometer specifications. ....	37
Table 2: The difference between the peaks of the different samples along with their respective bandwidth. ....	48
Table 3: Cross-Correlation table showing the correlation between the averages of the different samples. ....	50

# CHAPTER 1: INTRODUCTION

The food industry is a multi-trillion dollars industry that is directly related to the health and wellbeing of all people on Earth. Food safety and quality monitoring are considered paramount and considerable effort is being placed in their continuous improvement. The world health organization (WHO) estimates that food contamination causes the illness of at least 1 in 10 persons every year (approximately 600 million persons), and 420 000 die as a result (Food safety, 2019). According to the WHO, 220 million children contract diarrheal diseases due to unsafe food and 96 000 die each year (Davies, 2015).

There exist numerous developments in the field of food quality monitoring as researchers are constantly finding new methods and techniques to better, and quicker, detect food spoilage while optimizing food quality and shelf life. Almost all the traditional methods of measuring meat quality require the destruction of the sample being tested. Hyperspectral imaging is proving to be a pioneer in this field as the number of papers being published concerning hyperspectral imaging application in the food industry in the last 20 years is quickly increasing to exceed 200 papers per year in the 2010's (Huang, Liu, & Ngadi, 2014). This technique is the focus of this thesis as it possesses great potential when compared to other methods. Applying hyperspectral imaging in food presents a large amount of benefits, mainly the non-destructive, swift, remote, and accurate measurement, while also the possibility to incorporate this method in factory production lines is considered a real asset.

Hyperspectral imaging (HSI) is based on the concept of measuring light reflectance, which determines the amount of reflected light when hitting an object. Different materials absorb and reflects light in different ways. However, objects of the similar material reflect light in a similar fashion. This allows the classification, analysis and processing of hyperspectral data in many fields other than food which include agriculture, biology, astronomy, surveillance among others.

Before analyzing hyperspectral imaging, chapter 2 begins by defining the concept of digital images and explains how an image, composed of pixels and numbers, can be visible to human eye (visible spectrum) and contain other information that are also invisible. To make this separation,

the electromagnetic spectrum was defined and explained, and the bandwidths on which hyperspectral imaging is applied. Then, a thorough definition of HSI was presented, showing its applications, benefits.

Chapter 3 discusses the state of art of hyperspectral imaging in food monitoring. It lists several articles and papers that were published in journals and presented in conferences. The methods used in past research are explained and the promising and accurate results of applying hyperspectral imaging are shown.

In chapter 4, the detailed experimental setting of this research is presented showing the techniques that were used and the results it yielded. Finally, conclusions were drawn in chapter 5.

# **CHAPTER 2: LITERATURE REVIEW**

## **2.1 Introduction**

This chapter begins by defining and explaining digital images and their color models. Then, color bit depth is mentioned and examined. Also, the electromagnetic spectrum is discussed. In addition, the different methods of food detection are listed and explained. Finally, the concept of hyperspectral imaging is defined, its applications listed, and its benefits detailed.

## **2.2 Digital Images**

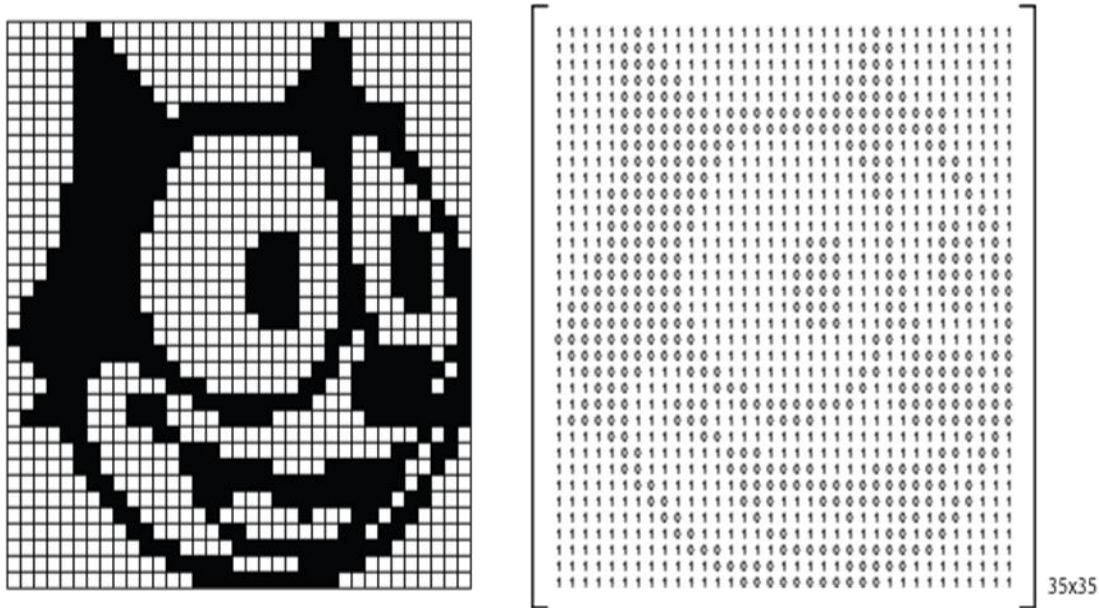
A digital image can be best defined as :" an image composed of picture components, also referred to as pixels, each with finite, discrete quantities of numeric representation for its intensity or gray level". (Gonzalez, 2018)

A digital image represent real image as a set of numbers that can be stored and processed by a digital computer. In order to convert images into numbers, they are divided into pixels (picture elements). Each pixel contains a number, or a small set of numbers, describing certain property such as the intensity of the light in the pixel (brightness) or the pixel's color. Then, these numbers are entered in an array that has rows and columns corresponding to the pixel' vertical and horizontal positions in the image (Digital Images, 2020).

Digital images have several basic characteristics. One is the type of the image. In its simplest form, only the intensity of light that is absorbed by the pixel is recorded in a black and white image. Meanwhile, A color image either has three colors, commonly known as RGB (Red, Green, Blue) model that is used in computer monitors and scanners, or four colors, represented by CMYK (Cyan, Magenta, Yellow, black) model which is dominantly used in color printers. There exist non-optical images such as ultrasound or X-ray the record the intensity of sound or X-rays. Image resolution is indicated in the number of pixels per inch (ppi) for digital screens, or in the number of dots per inch (dpi) for print papers. Images with higher resolution are generally more detailed. The resolution in a computer monitor is typically around 100 ppi, while that of a printer range from 300 dpi to more than 1200 dpi (Digital Images, 2020). This results in a much better image in

print than on a monitor. Figure 1 shows a simple, 1-bit, 35x35 grayscale image where each bit value equal to 1 is replaced by a white square whereas bits equal to 0 are replaced by a black one. It results in the schematic shown below.

*Figure 1: An example of a simplified (1-bit) grayscale digital image*



There are a number of ways to represent digital images. The most basic imaging type is grayscale imaging that uses a single color (black) with varying degrees. More complexing, there is the three-color imaging system using mainly the RGB system. Alternatively, but less widely used, there is the CMYK system, which uses four colors to represent digital images.

### 2.2.1 Grayscale Imaging

A grayscale (or graylevel) image uses shades of gray as colors. What differentiates such images from any other kind of color image is that each pixel contains considerably less information. Grayscale images are commonly and sufficiently used for various tasks such as face detection which does not necessitate using color images that are more complicated and harder-to-process. (Johnson, 2006)

In a greyscale image, each pixel stores a single value containing the amount of light, so, it only carries intensity information. Grayscale images are considered monochromatic, whose contrast ranges from the color black as its minimal intensity to white as its maximal intensity. (Johnson, 2006)

Grayscale images can result from measuring the intensity of light in each pixel based on a particular weighted combination of wavelengths (or frequencies), and can be captured as a single frequency (or a very narrow range of frequencies). These frequencies can originate from the whole electromagnetic spectrum (e.g. infrared, visible light, ultraviolet, etc.).

Below is an example of a digital image many intensities of the color black.

*Figure 2: An example of a grayscale image.*



### **2.2.2 RGB Imaging**

The RGB color model is considered an additive color model where the three colors red, green, and blue light are added together in different ways to produce a broad array of colors. The model is called RGB according to the initials of the three additive primary colors. This model follows the principle of additive mixing: colors begin from pure black until red, green and blue light is begins to add up to brighten it and create millions of possible colors. (Hirsch, 2004) When red, green and blue light is mixed at equal intensity, they create pure white. In other words, when 100% of each color are mixed, it creates white light. When 0% of each color is combined, no light is

generated, creating black. Color images can be represented by three matrices. Each of the three matrices represent a color and specifies the amount of red, green and blue that makes up the image. (RGB, 2019)

The RGB color model is primarily used for the sensing, representation, and display of color images in various electronic systems display, such as smartphones, televisions and computers, though it can also apply in conventional photography. The RGB color model concept started before its electronic applications since it gives an explanation of human perception of colors.

The RGB model applies differently in each device and can be considered a device-dependent color model as different devices detect or display a given RGB value in a diverse manner, since the color elements like phosphors or dyes and their response to each red, green and blue level vary between different manufacturers, and can even differ in the same device as it ages. Thus, color management systems are essential to manage the RGB value across devices.

RGB models takes its input and sends its output to different devices. Input devices typically include video cameras, digital cameras, and image scanners. While output devices commonly involve various sets of television technologies such as LCD, plasma, OLED and others, in addition to computers and mobile phones displays, and video projectors. It should be noted here that color printers are not RGB devices but rather use the CMYK color model. (RGB vs CMYK, 2019)

The number of colors that can be produced by the RGB model varies according to how many values can be used for the three colors of red, green, and blue. This refers to the “color depth” which is measured in bits. The 24-bit color is the most common color depth model and includes eight bits for each of the three colors totaling in 24 bits. 8 bits for each color provides  $2^8$  equaling 256 possible values for red, green, and blue. Multiplying this value (256) for each of the three-color matrix gives a total of 16,777,216 colors.

As shown below in figure 3, each pixel is represented by 3 values; that is the amount of red, green and blue. A digital image can be considered as collection of three matrices, each matrix representing the amount of the basic colors that compose this model.

*Figure 3: An example of a digital image by three color matrices.*

	165	187	209	58	7	
	14	125	233	201	98	159
253	144	120	251	41	147	204
67	100	32	241	23	165	30
209	118	124	27	59	201	79
210	236	105	169	19	219	156
35	178	199	197	4	14	218
115	104	34	111	19	196	
32	69	231	203	74		

---

### **2.2.3 CMYK Imaging**

The second most used color model is the CMYK model, which is a subtractive color model mainly used in color printing. CMYK refers to the four ink plates utilized in most color printing systems. These plates are cyan, magenta, yellow, and key (black) (Campbell, 2000).

The CMYK model working principle dictates partial or entire masking of colors with varying degrees, on a light background usually chosen white. The ink reduces and alters the light that would otherwise be reflected. This model is considered subtractive since used inks "subtract" the three colors of red, green and blue from white light. Red light subtracted from white light results in cyan, white light minus green leaves magenta, and blue taken from white light yields yellow. This is known as subtractive mixing. All colors begin as plain white, and each layer of ink reduces the initial brightness to create the desired color. When all colors are combined, they yield pure black (RGB vs CMYK, 2019).

As opposed to the RGB model, where the color white is the "additive" combination of all other colors and black is the absence of all other lights, the CMYK model considers white as the natural color of the paper or other background, while black results from the full mixing of the three colored inks. As producing the color black requires three colors that may be costly, to save

cost on ink, and to produce deeper black tones, black ink is used instead of the combination of cyan, magenta, and yellow.

Based on the working principle of CMYK model, it can be seen that, it is only viable for any image or picture that will be physically printed, not viewed on a screen. Its uses include any printing with ink or paint such as business cards, billboards, posters, brochures, etc.

## **2.3 Color Bit Depth**

Bit depth specifies to the color information stored in an image. Bit depth, technically, describes the number of color values per channel - Red, Green, and Blue. As bit depth of an image increase, the colors it can store increase as well. The simplest image, having only 1 bit, can only show two colors, black and white. That is because the one bit can only store one of two values, 0 (white) and 1 (black). An 8-bit image can display 256 possible colors, while a 24-bit image can show more than 16 million colors. This does not mean that the image necessarily uses all the colors, but that it can instead specify colors with that level of precision. (Bit Depth, 2019)For a grayscale image, bit depth indicates the number of unique shades of gray it can display. Images having higher bit depths, can display a greater amount of colors since there are more combinations of 0's and 1's available. As the bit depth increases, the file size of the image also increases because more color information must be stored for each pixel in the image (What is bit depth?, 2018).

Each pixel color in a digital image is a result of the combination of the three primary colors: red, green, and blue. Every primary color can be referred to as a "color channel" and its range of intensity values are specified by its bit depth. The bit depth for each color is often referred to as the "bits per channel". The "bits per pixel" (bpp), on the other hand, is the summation of the total bits in all the color channels and indicates the total number of colors that can be displayed at each pixel. (Sullivan, Ohm, & Wiegand, 2013)

As mentioned in the previous section, most color images from digital cameras possess 8-bits per channel using a total of eight 0's and 1's which results in 256 different intensity values for each primary color. When all three primary colors are mixed at each pixel, this allows for as many as 16,777,216 different colors, what is referred to as "true color."

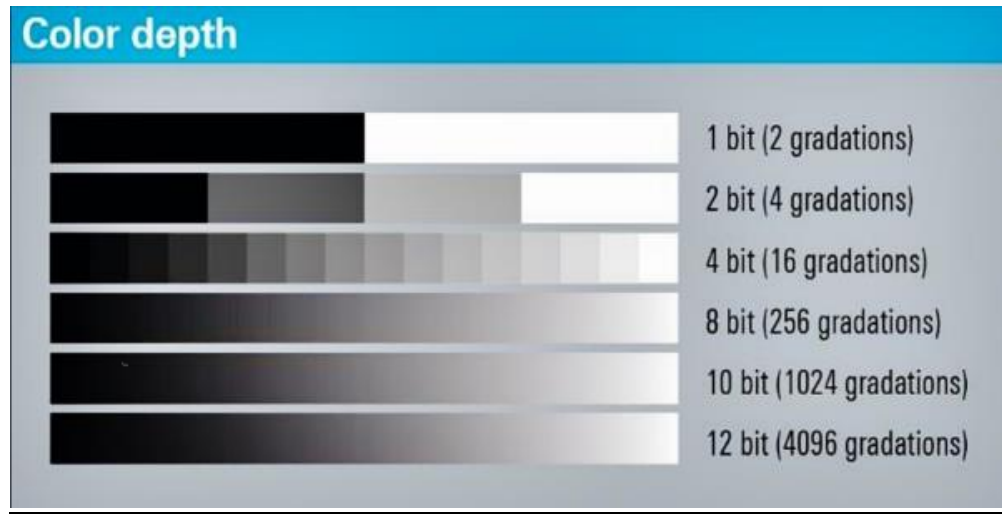
In an RGB, 8-bit color system, three color matrices exist. Each element in these matrices determine the color intensity of the pixel. These elements are integer numbers between 0 (indicating the color of minimal intensity) and 255 (indicating the color maximum intensity).

As the following results show, slight increases (from 8 to 10 bits) in the number of bits per color channel results in exponential increases in the total number of colors that can be represented in an RGB color model:

- 8 bits per color channel: 16,777,216 total colors
- 10 bits per color channel: 1,073,741,824 total colors
- 12 bits per color channel: 73,876,521,536 total colors
- 14 bits per color channel: 4,398,046,511,104 total colors
- 16 bits per color channel: 281,474,976,710,656 total colors

Figure 4 shows number of bits effect on color depth gradations for a grayscale image. As it can be observed, as the number of bits increase, the number of gradations also increase, and as a result the smoothness of the transitions between the black and white increase as well.

*Figure 4: The number of bits effect on color depth gradations.*

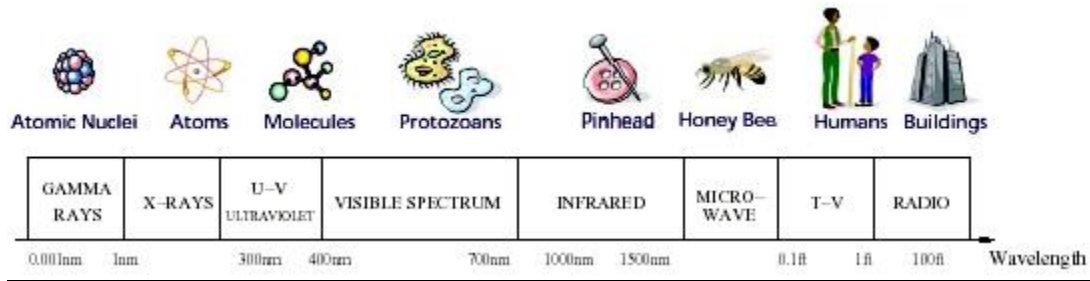


## **2.4 Electromagnetic Spectrum**

The electromagnetic spectrum consists of the range of frequencies, often called the spectrum, of electromagnetic radiation along with their respective wavelengths and photon energies. Radiation can be defined as: “the emission or transmission of energy in the form of waves or particles through space or through a material medium”. The spectrum covers electromagnetic waves with frequencies ranging from less than one hertz to above  $10^{24}$  hertz, relating to wavelengths from thousands of kilometers down to less than a nanometer. (The Electromagnetic Spectrum, 2013)

The electromagnetic spectrum comprises the span of all electromagnetic radiation and consists of several subranges, usually referred to as portions, and it includes: radio waves, microwaves, infrared, visible light, ultraviolet, X-rays, and gamma rays. There are no specific accepted boundaries between any of these adjacent portions, so the ranges have a tendency to overlap. Sorted by increasing wavelength, the electromagnetic waves are shown in the figure 5, and listed afterwards in details. (Augustyn, Bauer, & Duignan, 2018)

*Figure 5: The electromagnetic spectrum.*



### **I. Gamma radiation**

Gamma ray is a penetrating electromagnetic radiation originating from the radioactive decay of atomic nuclei. It possesses the shortest wavelength electromagnetic waves and so transmits the highest photon energy.

## **II. X-ray radiation**

Much more commonly known than gamma rays, x-rays have many applications in everyday life. X-rays have wavelength ranging from 0.01 to 10 nanometers, and are generally known for their ability to penetrate human skin and reveal images of the bones. Other applications of X-rays include security scanners commonly used in airports which detects the presence of metal.

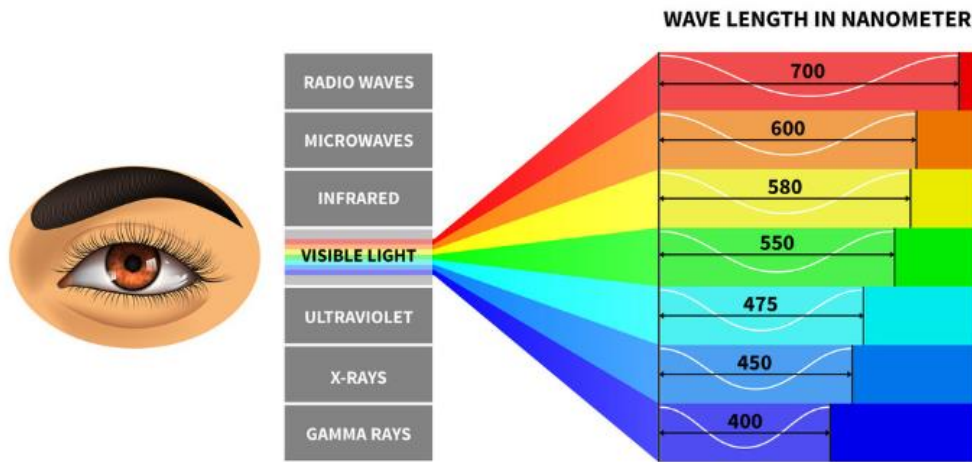
## **III. Ultraviolet radiation**

Ultraviolet radiation is emitted by the Sun and when absorbed by the human skin causes it to darken. Its wavelength ranges from 10 nanometers to 400 nanometers. Short-wave ultraviolet light damage DNA and sterilizes surfaces that it comes into contact with. Also, long exposure with human skin can cause skin cancer. (The Electromagnetic Spectrum, 2013)

## **IV. Visible light**

This subrange is called visible since it is the portion of the spectrum that is visible to the human eye. It spans from wavelength of 400 to 700 nanometers. As shown below visible light is composed of several colors that range from blue (400 nm) to red (700 nm) which are at both ends of the spectrum subrange. The most commonly used color model is the RGB color model previously discussed.

*Figure 6: Visible light composition of the electromagnetic spectrum.*



## **V. Infrared radiation**

Infrared light possess light with wavelength longer than those existing in the visible range. They range from the edge of the red edge of the visible spectrum (700 nm) to approximately 1 millimeter. Thermal radiation is emitted in the infrared range making night vision possible through specially equipped devices. Of special interest in hyperspectral imaging is the range called Short Wave Infrared (SWIR). It comprises nonvisible light of wavelength between 1400 and 3000 nanometers.

## **VI. Microwave radiation**

Microwaves are a form of electromagnetic waves that range from 1 millimeter in wavelength to about of 1 meter. The most known application of microwave radiation are electronic appliances used to heat food. Microwaves travel only by line of sight routes. They are also heavily used in point-to-point telecommunications such as navigation systems (GPS) and Radar.

## **VII. Radio waves**

Radio waves have frequencies ranging from as high as 300 gigahertz to as low as 30 hertz. They are not emitted by natural sources but are rather generated by man-made transmitters and received using antennas by radio receivers. Some very widely used modern technology include: radio navigation systems, wireless computer networks and communications satellites.

## **2.5 Methods of Detecting Meat Spoilage**

Traditional methods to assess freshness of food rely on human senses: that involves looking at it to detect any change in color, smelling it and finally touching it to sense any sticky or slimy substance. Although they are essential, they provide no quantitative data of spoiled food. Thus, the food industry developed the use of expiry dates that are written on the labels of different categories of foods. These expiry dates take into consideration the process of spoilage of different types of

food and approximates the number of days that they can be kept in storage before they should be thrown away.

Although this method is the safest and the most applicable to the mass production of food, it sometimes causes the wasting of food that is still eatable. To maximize the amount of time food can be used, while also maintaining acceptable levels of food safety, researchers are continuously developing new alternative techniques to detect the spoilage of food, these methods include the use of biosensors, hypoxanthine detection in fish products, gas detection using chemiresistors and the use of optical sensors.

### a) Hypoxanthine Detection

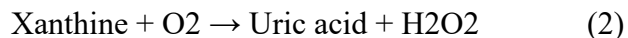
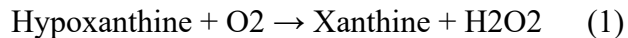
As the food industry grows and continuously improves, an increased demand is created for long-term storage and preservation of food. This, in turn, resulted in a need to develop methods that can efficiently track and preserve the freshness and safety of food throughout all the stages of the shelf life of the product. Smart sensors and labels that can possibly be attached to the food package can be extremely helpful in the constant monitoring of the product status. These can be built and designed to measure indicators of freshness and provide an “index of quality” of the produce in real time, measure temperature changes, or identify the existence of harmful substances. (Mustafa & Andreescu, 2018)

When protein-based food such as meat, fish, or poultry begin to degrade, different spoilage indicators can show protein breakdown, and protein adenosine triphosphate (ATP) decay. The pace of degradation depends on the type of product, storage temperature, feeding manners, and harvesting techniques. The status and quality of food can be better assessed by quantitative measure markers of degradation through different chemical or biological reactions. (Mustafa & Andreescu, 2018)

For example, in fish products, a crucial freshness indicator is hypoxanthine, which is produced by the metabolic degradation of ATP.

Detection of hypoxanthine by XOD (xanthine oxidase) involves various reactions and steps:

Step 1: hypoxanthine is oxidized to xanthine, which is then oxidized to uric acid as shown in following reactions:



Step 2: The H<sub>2</sub>O<sub>2</sub> produced in reaction (2) shown above, undergoes what is called, a Fenton reaction, which is defined as a catalytic process that converts hydrogen peroxide (H<sub>2</sub>O<sub>2</sub>) into a highly toxic hydroxyl radical (OH), in the presence of Fe<sup>2+</sup>.

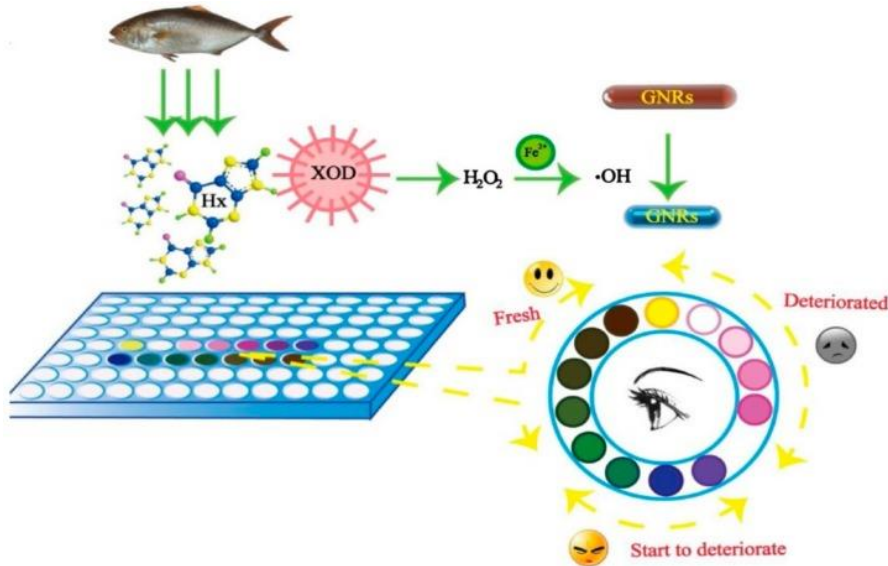
Step 3: Gold nanorods (GNRs) present in the multicolor sensor system, reacts to the hydroxyl radicals (OH), and thus forming a vivid color change.

Step 4: Different colors, including reddish brown, gray, green, blue, purple, pink, and yellow, are displayed depending on the concentration of hypoxanthine.

The below figure shows a schematic detailing the hypoxanthine detection process. As can be seen, each range of colors indicates a different status of the fish. Colors ranging from dark green to brown indicate fresh fish, whereas other colors such as green, blue, and violet signify that the fish is about to deteriorate. Finally, light colors such as yellow, white, and different shades of pink signal a deteriorated fish. (Mustafa & Andreescu, 2018)

The use of visual color indices makes this technique minimally confusing, user friendly, and possibly usable by many people.

Figure 7: A schematic detailing the hypoxanthine detection process.



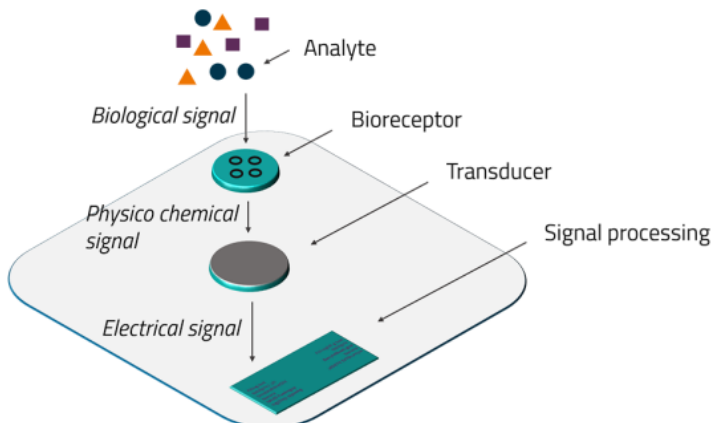
## b) Biosensors

Another example of developing methods of detection is the use of biosensors. Biosensors are devices which use a living organism or biological molecules, such us enzymes or antibodies, to detect the presence of chemicals and pathogenic bacteria.

Pathogenic bacteria, such as Escherichia coli and Salmonella, are one of the main causes of diseases and foodborne outbreaks in many countries in the world. Therefore, rapid detection of these bacteria can reduce diseases and thus improve the quality of food.

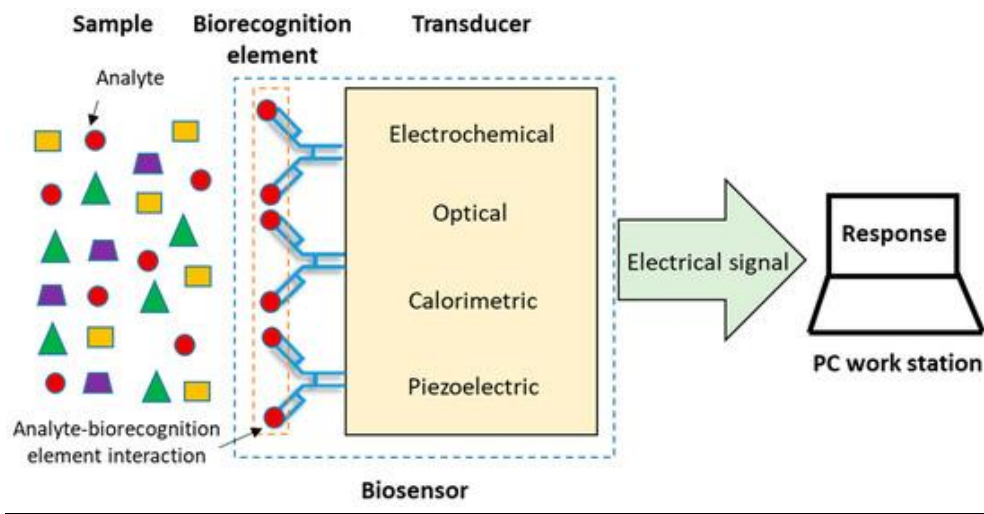
Biosensors have many benefits due to their portability, mobility and potential for onsite detection without the need to transport samples to the lab. They may also be used on many inactive pathogens. As the figure below shows, a biosensor is mainly composed of a bioreceptor, a transducer and a signal processor. The bioreceptor receives the biological signal that is emitted by analytes, which then sends a physicochemical signal to the transducer, that in turn analyses the received signal and sends an electrical signal to the signal processor. The signal processor, which can be located on a portable computer, shows the final results of the assessment of the food that has been tested.

*Figure 8: The structure of a biosensor.*



**Structure of a biosensor**

Figure 9: A schematic showing the basic elements of a biosensor.



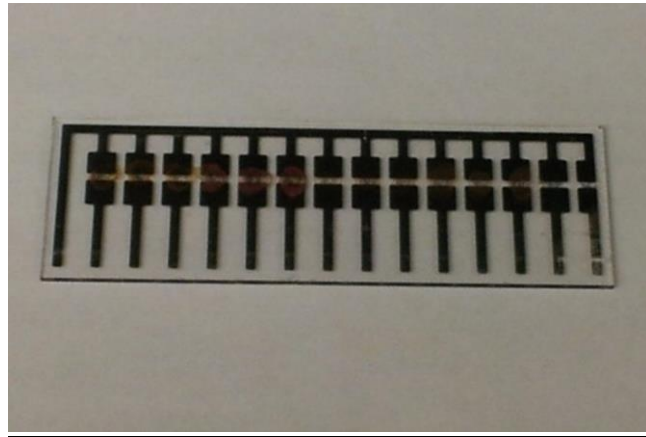
### c) Gas Detection with Chemiresistors

The Massachusetts Institute of Technology (MIT) have announced that its researchers, led Professor Timothy Swager, have developed a portable and an inexpensive sensor system, mainly made of chemiresistors, which can rapidly detect the gas released by spoiled food. (Detect Food Spoilage with Sensors, 2017)

A chemiresistor can be defined as: “a material that changes its electrical resistance in response to changes in the nearby chemical environment”. Chemiresistors are a class of chemical sensors that rely on the direct chemical interaction between the sensing material and the analyte. The sensing material and the analyte can interact by covalent bonding, hydrogen bonding, or molecular recognition.

The sensor system electrical is composed of lines of carbon nanotube compounds called metalloporphyrin. Metalloporphyrin interacts with amines, which is a compound emitted by spoiled meat. This binding increases the resistance of the carbon nanotube, causing as a result a change in the electrical signal transmitted by the sensor. The sensors use near-field communication (NFC) tags to communicate with smartphones with NFC capability, and notify them in case any alteration in the circuit has been and thus resulting in the detection of the meat decay. (Detect Food Spoilage with Sensors, 2017)

*Figure 10: The device composed of modified carbon nanotubes.*



#### d) **Optical Sensors**

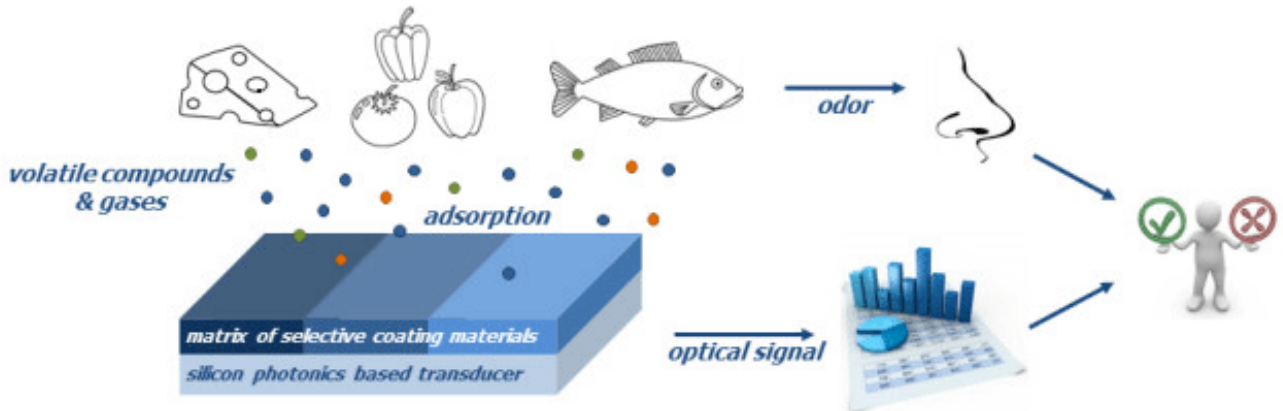
This research started in November 2013 and would run for four years. It is a joint collaboration between Ghent University, VU University and Radboud University, and is funded by IWT, a Flemish government agency for Innovation by Science and Technology. (Fletcher & Mullane, 2018)

An optical sensor, that uses volatile biomarkers coated on its surface, can monitor the quality of food inside a container and signals a warning in case of food spoilage. This sensor is the result of a joint cooperation between three universities (VU University, Ghent University, and Radboud University) and is funded by a Flemish government agency called IWT.

The optical sensor operates as follows: when the volatile components are exposed to the sensor's biomarkers, their refractive index changes. This change is detected by the infrared (IR) light that is directed towards the sensor, causing a wavelength change (shift) of the IR light reflected by the sensor. Following this shift, the volatile components and their concentration can be determined inside the container using a certain mathematical model (Fletcher & Mullane, 2018).

Figure 11 shows a simple schematic showing the operating principle of the optical sensor.

Figure 11: A schematic of the operating principle of the optical sensor.



## 2.6 Hyperspectral Imaging

### 2.6.1 Hyperspectral Imaging Definition

Hyperspectral imaging involves collecting and processing information in the form of data or images from across the electromagnetic spectrum. Hyperspectral image processing relies on computer algorithms and programs to extract, store and process information from the bands in the visible near-infrared (VNIR) or near-infrared (NIR) hyperspectral images that can be used for several information processing and data mining tasks that include analysis, classification, target detection, and pattern recognition. (Chang, 2003)

Certain objects possess a 'fingerprint' in the electromagnetic spectrum known as spectral signatures. These 'fingerprints' are unique and allow the identification of the materials that constitute the scanned object. (Bosoon, 2015)

The boom in the field of hyperspectral imaging was due to advancing technology which allowed the shift from large-size, fragile, and costly laboratory spectrometers to being operated in real time satellites, unmanned aerial vehicles, and mobile handheld units.

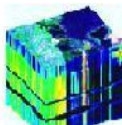
The techniques for hyperspectral image processing are heavily used in the optics domain. The digital signal processing deals with one-dimensional signals (time or frequency domain signals) which usually involves small part of an image called pixels, whereas the digital image

processing deals with multidimensional (space- and space-time-domain) signals such as images and videos.

Human vision perceive color of visible light in largely three bands: long wavelengths - observed as red, medium wavelengths - observed as green, and short wavelengths - observed as blue. Spectral imaging on the other hand, segment the spectrum into considerably larger number of bands. Multispectral imaging involves discrete, spaced bands of the spectrum, with each band representing an interval of bands. In hyperspectral imaging, hundreds of bands are measured and can be considered as continuous and of a relatively high wavelength resolution covering a wide range of wavelengths (Gibbons, 2014).

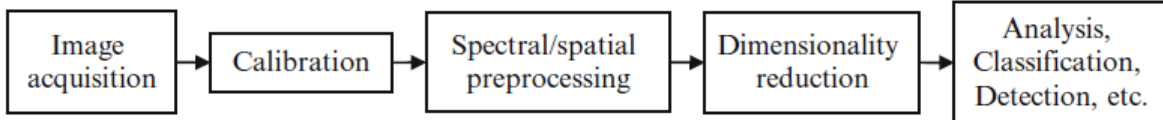
Figure 12 illustrates the main difference between the different types of imaging as to the variation in the number of bands.

*Figure 12: Differences in number of bands of the different type of imaging.*

				
Grey Scale	Color	Multispectral	Hyperspectral	Ultraspectral
1	3	2~30+	30~300+	300+
Single	Discrete	Discrete	Continuous	More Continuous

Typically, hyperspectral image processing workflow involve several steps. It begins by the image acquisition, then calibration and atmospheric correction which is used only for remote sensing, then creation of a reflectance data cube, then it moves to dimensionality reduction which include feature extraction and selection, and finally concludes with analysis, classification or any other data processing technique that may be used. Figure 11 shows the steps that are involved in the typical hyperspectral image processing workflow (Bosoon, 2015).

*Figure 13: The hyperspectral image processing workflow typical steps.*



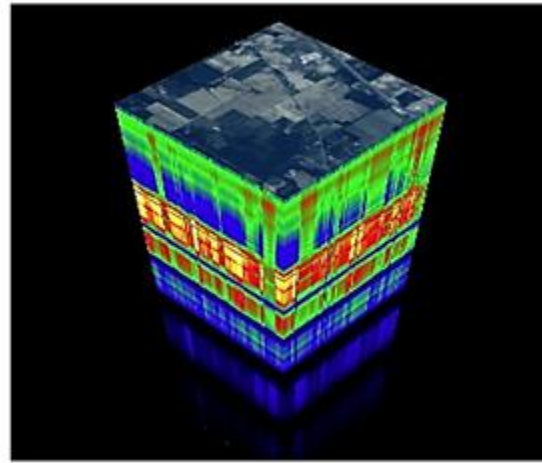
## **2.6.2 Hypercube**

A term that is heavily used in the hyperspectral imaging field is that of a ‘Hypercube’. Hypercubes encompass a set of large number images stacked together forming a figurative cube. Hyperspectral sensors collect information from each bandwidth as a set of images. Each spectral band, which is wavelength range of the electromagnetic spectrum, is represented by an image. These ‘images’ combine to construct a three-dimensional ( $x, y, \lambda$ ) hyperspectral data cube, where  $x$  and  $y$  represent two spatial dimensions of the object being scanned, and  $\lambda$  represents the spectral or bandwidth dimension (representing a range of wavelengths) (Bosoon, 2015).

The cube ‘thickness’, i.e. the number of images that it comprises, is heavily related to the hyperspectral imaging sensor resolution. This means that as the resolution becomes finer, the amount of data in the hypercube increases, and the sensor is considered to be more precise. Spectral resolution is the width of each band of the spectrum being captured. If the scanner measures numerous narrow frequency bands, objects can be detected even if captured in a couple of pixels. However, spatial resolution is an important factor that should be considered. If the pixel size is too large, then many objects may be captured in the same pixel and they can be difficult to identify. If the pixel size is too small, then the energy or light captured by each sensor cell is small, resulting in a decreased signal-to-noise ratio and thus reducing the reliability and accuracy of the sensor.

A figurative illustration of a hypercube is shown in figure 14 below. This cube does not necessarily exist in its current form but is shown to highlight how an image of plain fields as shown in the visible range, can often contain a great amount of seemingly bizarre data in other bandwidths, that are outside the visible range.

*Figure 14: An example of a hypercube.*



The following are examples of hyperspectral signals taken from different elements of nature. As can be seen, each material possesses a totally unique signature and that the amount of reflectance greatly varies with each bandwidth. As bandwidth increase, some signature's reflectance increase, some decrease, while others fluctuate.

*Figure 15: An example of hyperspectral signal signature of Soil.*

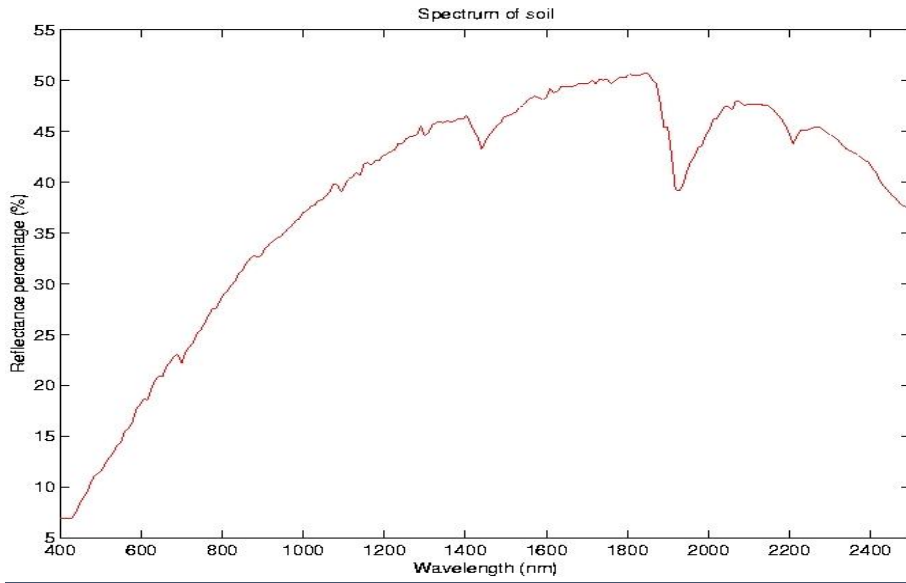


*Figure 16: An example of hyperspectral signal signature of Rock.*

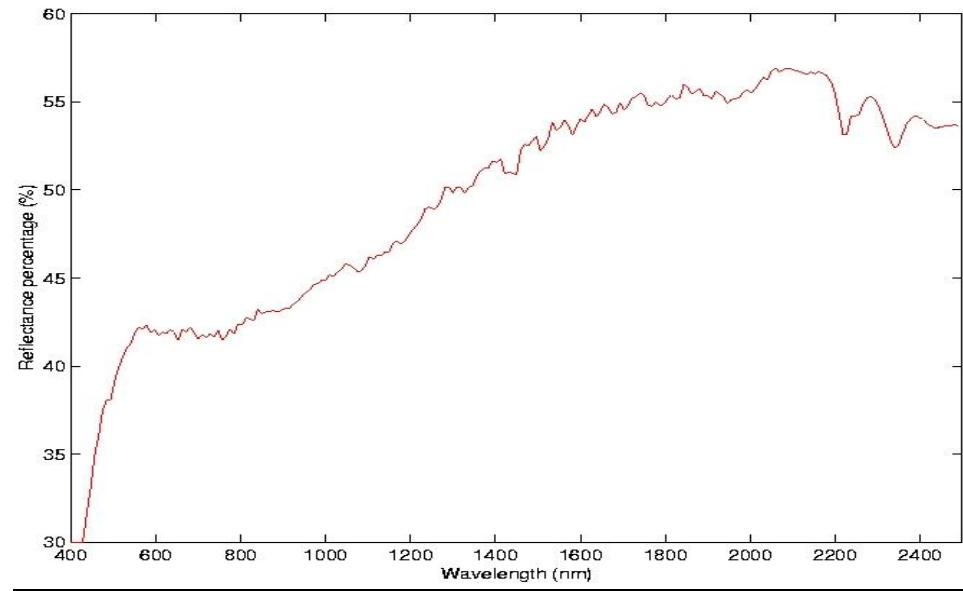


*Figure 17: An example of hyperspectral signal signature of Water.*

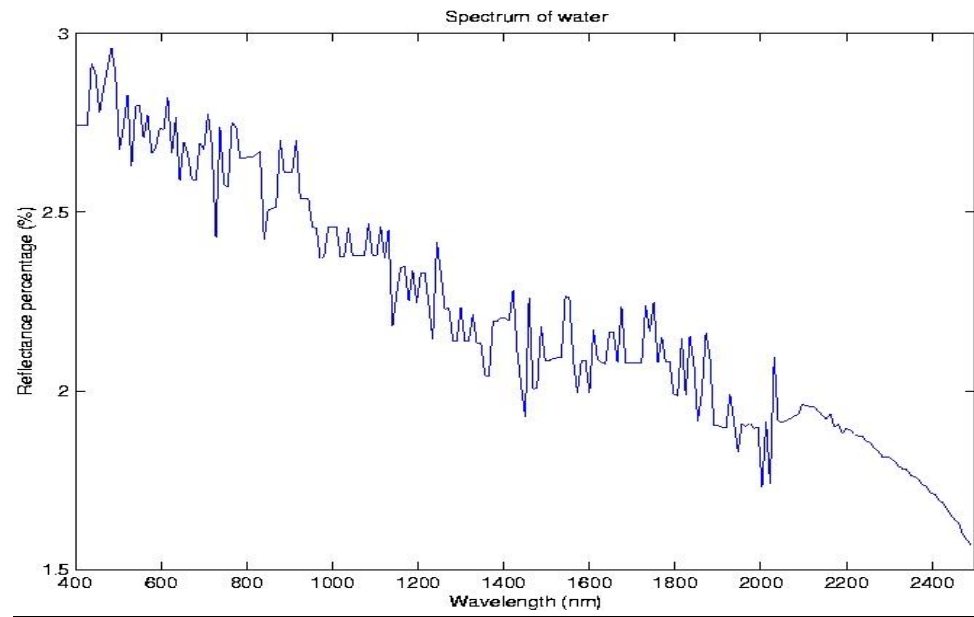
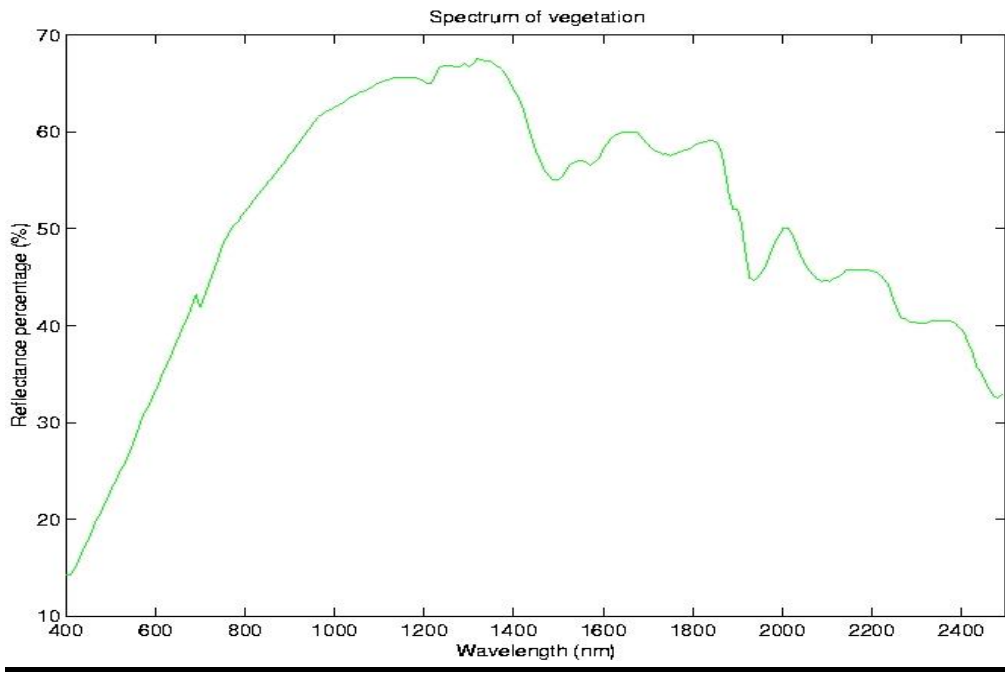


*Figure 18: An example of hyperspectral signal signature of Vegetation.*



### **2.6.3 Hyperspectral Imaging Applications**

Hyperspectral imaging is being widely used in various fields ranging from satellite remote sensing to forensic science. As technology evolves, hyperspectral imaging benefits outweighs its drawbacks and additional applications are being discovered. The following are some of the applications that are adopting the hyperspectral imaging technology.

#### **A. Satellite Remote Sensing:**

Satellite remote sensing has become a very popular technology being used to distinguish between earth surfaces features as each feature possess a unique spectrum band. This allows monitoring of oceans, plains, mountains and other areas that may be inaccessible by civilization. (Important Applications of Hyperspectral Image, 2016)

Hyperspectral imaging satellite remote sensing can either be active or passive. Active remote sensing indicates that the satellite emits the signals and receives their reflections, whereas passive remote sensing involves receiving the signals reflecting off objects that were previously emitted by the sun's natural sunlight. This allows the modeling and analysis of the earth' surfaces allowing differentiation of objects that were previously undifferentiated in multi spectral imaging as a result

of their relatively low spectral resolution. Figure 19 shows a simplified schematic of the satellite remote sensing where figure 20 reveals the main difference between active and passive remote sensing.

*Figure 19: The main difference between active and passive remote sensing.*

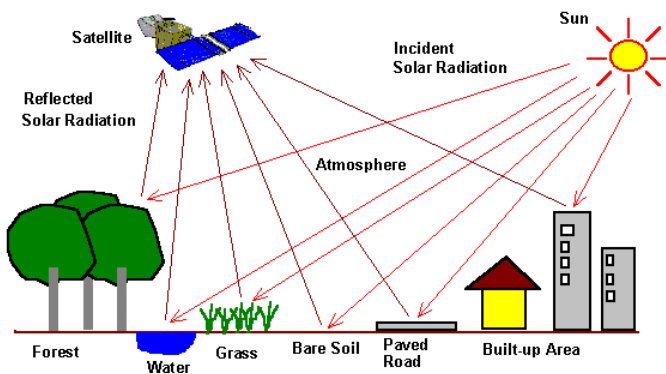
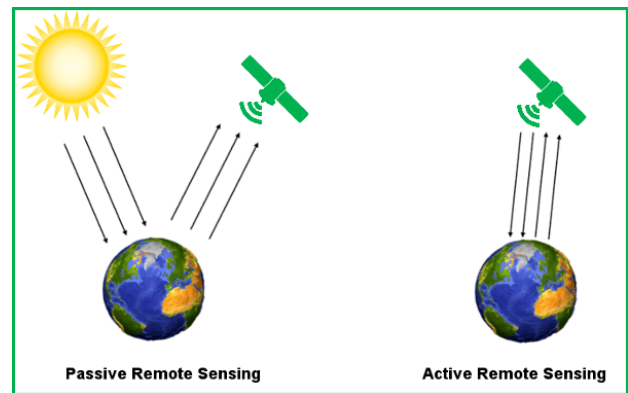


*Figure 20: A simple schematic of the satellite remote sensing process.*



## 2. Biotechnology:

Biotechnology refers to the use and manipulation of living organisms in the purpose of developing products in the biology field. Hyperspectral technology plays a crucial role in this endeavor. It helps acquire rich data that can be used in the laboratory in tasks that include cell biology, wound analysis, among many other tasks. Also, hyperspectral imaging helps in identifying tumor margins during certain brain surgery, also in screening for several of neurodegenerative diseases, and assists in identifying cognitive impairment.

In addition to the above-mentioned benefits, this imaging technique provides quantitative diagnostic information about tissue anatomy since the reflected, fluorescent, and transmitted light from tissues changes in certain medical conditions (Important Applications of Hyperspectral Image, 2016).

Hyperspectral Imaging developed an appeal in the field of medicine and biology as it considered a non-contact, rapid, non-ionizing, and considerably less invasive technology.

### **3. Environmental Monitoring:**

Hyperspectral imaging is often used for monitoring and tracking changes in the environment. Its applications include but is not limited to detecting surface CO<sub>2</sub> emissions, mapping hydrological formations, and tracking pollution levels. In addition, this technology is helpful in mapping sea grass beds and coral reefs. Collected data help establish sea grass bed location and extent, approximate its photosynthetic production, and assist in monitoring environmental changes over time relating to issues such as deterioration of the sea life and pollution of the air and the increase in its CO<sub>2</sub> content.

Agriculture is another field being heavily affected by the use of hyperspectral imaging, especially in overseeing the development and health of crops, detecting the chemical composition of plants, identifying the nutrient and water status of wheat in irrigated systems, and rapidly monitoring the application of pesticides to individual seeds for quality control (Chamberland, Farley, Vallières, & Belhum, 2005).

Another application of hyperspectral imaging in agriculture is in fighting the spread of bovine spongiform encephalopathy (BSE), also known as the mad-cow disease, by detecting the presence of animal proteins in compound feeds.

### **4. Food:**

In the food processing industry, hyperspectral imaging provides countless applications which have the potential to revolutionize the industry. It could detect bruises in apples, assess the freshness of fish, allows the inspection citrus fruit inspection, measure distribution of sugar in melons, and many other tasks. In addition, blemishes and bruising under the skin of many fruits and vegetables can be detected (Bosoon, 2015).

One of the most important applications of HSI involves defining the ripeness and chemical properties of the fruit independent of its color and size, as well as detecting foreign materials that are invisible to traditional cameras like wood, paper, plastic, metal, or insects. This ensures a better quality, ripe products having an optimized shelf life, and thus reducing losses and waste.

Using hyperspectral imaging on production lines digital sorters is being done in many factories. The software of the sorter compares collected hyperspectral images to user-defined

accept or reject thresholds, and then the ejection system automatically removes the detected foreign material or defects. For example, in the nut industry, specialized systems enable the removal of stones, shells and other possible foreign material from walnuts, pistachios, almonds, peanuts and other kind of nuts. In this case, the cost of the technology is justified by the improved product quality, low false reject rates and the capability to handle high incoming loads (Hyperspectral Imaging Applications, 2019).

## **5. Forensic Science:**

In forensic science, hyperspectral imaging technology is providing a tremendous amount of benefits. It can be used in gun powder residue detection, fingerprint enhancement, identifying blood stains, analyzing paint marks in hit-and-run cases. For example, hyperspectral imaging can help differentiate between dark marks and bloodstains which is very critical in any crime case. It can easily and quickly identify blood stains in a crime scene. It also can determine the age of a blood stain without involving any chemicals. In this way the blood spatter is neither diluted nor altered but scanned remotely.

In addition, hyperspectral imaging allows the examination of gunshot residue which is considered delicate evidence. Traditional ways of detection involve a forensic investigator applying chemicals for visualization, which can alter the pattern used for reconstruction and determining valuable information such shooting distances and angles. As a result, valuable information may be destroyed. On the other hand, Hyperspectral imaging provide a fast, contactless tool for detecting the presence of the gunshot residue at a scene and visualizing the shooting patterns.

Hyperspectral imaging can provide the analysis of paint marks in hit-and-run cases. Often in hit and run cases, paint marks can be visible on the scene which gives crucial information on the vehicle that escaped the scene. However, paint analysis requires a delicate procedure involving microscopes and sample preparation. Using hyperspectral imaging, paint spectra help in narrowing down the possible models of the car in very short time. Finally, forensics can use hyperspectral imaging in determining the age of a bruise accurately. Fraudulent documents can also be identified in the laboratory without the need to destroy the sample

In addition to the previously discussed applications, there exists numerous others in many domains such as intelligence surveillance, pharmaceuticals and astronomy.

## **2.6.4 Benefits of Hyperspectral Imaging in Food Application**

Hyperspectral imaging systems possess many advantages when compared to classical chemical and physical analytical methods in the food industry. These benefits make a strong case for the use of the technology in the industry especially as its cost is continuously decreasing and its use is becoming more user-friendly. They include the following:

- Nondestructive method of inspecting and monitoring of food quality, as it doesn't require contact with the food while also avoiding its destruction or contamination of the sample.
- Many important chemical bonds in food samples absorb light at wavelengths in the SWIR region (900 – 2500 nm) allowing the detection of elements like moisture content, protein and fat content.
- A short measuring time with decreased sample preparation.
- Chemical-free and passive measurement tool.
- Multiple attributes can be measured simultaneously as opposed to a single attribute in other measurement techniques.
- Reduced energy requirements and costs of process.
- Reduced sickness and food especially as traditional food expiry dates might not be reliable if the food has been improperly stored.
- Prolonging the shelf life of products since it provides more accurate information than the expiry date on food packets.
- A wide range of multi-constituent surface and sub-surface features identified by the spectral feature of the system.
- Detection of certain diseases and stains that exists under the skin of the fruit or vegetable and that are invisible to the human eye.
- Identification of certain chemical properties that may be due to the use of pesticides.
- Optimizing the quality of food by picking higher quality food based on certain criteria such as sugary content of strawberries or watermelons.

## **2.7 Conclusion**

This chapter discussed important concepts that help understand hyperspectral imaging, its definition, components, applications and possible benefits in the food industry.

Before getting to hyperspectral imaging, explaining the notion of digital images and image color models was very important, especially to those unfamiliar with the concept of bandwidths and wavelengths in the electromagnetic spectrum. Color bit depth is an interesting concept that broadened the discussion scope and finally, the listing and analysis of different methods of detection of food quality and spoilage, highlighted the focus on, and industry trends towards finding alternative and more efficient techniques of monitoring food quality, and the important role that hyperspectral imaging can contribute in this field. The next chapter, titled state of art: Past experiment and existing articles, will include a discussion of the studies and articles that have been published concerning the use of hyperspectral imaging in the food industry. It will show the great potential and exciting results that came out of numerous studies, which was the main motivation behind the research project being discussed in this report.

# **CHAPTER 3: STATE OF THE ART: PAPERS AND PAST RESEARCH**

## **3.1 Introduction**

This chapter's objective is to list and describe previous research involving hyperspectral imaging use in food monitoring. These researches include papers that have been discussed in conferences and journal articles and shows various applications of hyperspectral imaging in food groups such as beef meat, strawberries, milk, and pork fat.

## **3.2 Past Research**

The main focus in this section is on research papers that have specifically used hyperspectral imaging in the food industry. This technique is used in various other fields, and there exists numerous other techniques employed in the food industry, but it was opted to specifically include researches whose scope is similar to that of this research project.

### **3.2.1 Hyperspectral Imaging for Nondestructive Determination of Some Quality Attributes for Strawberry**

This study used hyperspectral imaging for the nondestructive determination of important attributes of strawberry. These attributes are considered important indicators of strawberries and include moisture content (MC), total soluble solids (TSS), and acidity (expressed as pH). Following the acquisition of spectral images, each fruit was cut into two equal halves. The first half was utilized for determining moisture content, and the second half was made as juice to measure its pH and its total soluble solids (ElMasry, Wang , ElSayed, & Ngadi, 2006).

Firstly, the moisture content was determined by forced-air convection using oven-drying method, whereas, a pH meter and a refractometer measured the strawberry juice's pH and total soluble solids respectively.

Secondly, the spectral data were analyzed using the partial least squares (PLS) analysis. The correlation coefficients ( $r$ ) was computed in a spectral range of 400–1000 nm for predicting

the three attributes of MC, TSS, and pH were 0.90, 0.80, and 0.87 with standard error of calibration (SEC) of 6.085, 0.233, and 0.105 and standard error of prediction (SEP) of 3.874, 0.184, and 0.129, respectively. Also, multiple linear regression (MLR) models were considered and their correlation coefficients ( $r$ ) for predicting MC, TSS, and pH were 0.87, 0.80, and 0.92 with SEC of 6.72, 0.220, and 0.084 and SEP of 5.786, 0.211, and 0.091, respectively. The results concluded that using a nondestructive technique is possible using hyperspectral imaging for measuring strawberry quality parameters (ElMasry, Wang , ElSayed, & Ngadi, 2006).

### **3.2.2 Line-Scan Hyperspectral Imaging Techniques for Food Safety and Quality Applications**

Qin et al, studied the effect of using the line-scan hyperspectral imaging technique for food safety and quality application in an article which was published in the Multidisciplinary Digital Publishing Institute (MDPI) in 2017. Line-scan hyperspectral imaging techniques have been deeply researched and developed for measuring physical, chemical, and biological properties of a broad range of food and biological materials. This technique was further used in food safety and quality evaluation, plant maturity and disease monitoring, raw material screening, food processing assessment, and equipment sanitation inspection (Qin, Moon, & Chao, 26 January 2017).

This study focused on online wholesomeness inspection of freshly slaughtered poultry carcasses on a high-speed commercial chicken processing line. Hyperspectral reflectance images were collected in 55 bands (389–753 nm) from the chicken carcasses that were moving at a speed of 140 birds per minute (bpm) by a sensing unit which consisted of lens, a spectrograph, and an EMCCD camera. Single-band 2-D spatial images were compiled from the acquired line-scan hyperspectral images for offline image and spectral analysis, such as region of interest (ROI) optimization and key band selection. By analyzing the two-band ratios, using 580 and 620 nm yielded the largest difference between the average ROI reflectance spectra of the wholesome chickens and the systemically diseased chickens. During continuous operation for over 100,000 chickens, the multispectral system achieved over 99% accuracy in identifying wholesome chickens and over 96% accuracy in identifying unwholesome chickens. The system can improve chicken product safety by preventing most unwholesome birds from entering the production line and by reducing the routine workload for food safety inspectors working in the chicken

processing plants (Qin, Moon, & Chao, 26 January 2017).

### **3.2.3 Advanced Applications of Hyperspectral Imaging Technology for Food Quality and Safety Analysis and Assessment**

Hyperspectral Imaging (HSI) has proven its capability in the quality and safety evaluation of fruit and vegetables, such as detecting contamination, bruises, surface defects, and measuring maturity stage. Wu et al, studied the effectiveness of using HSI in assessing food quality and concluded that by using algorithms such as linear discriminant analysis (LDA), quadratic discriminant analysis (QDA), stepwise discriminant analysis (SDA), and partial least squares discriminant analyses (PLS-DA), detection of insect damages in cucumber was more successful than manual inspection with an overall accuracy of 82–93% compared to 75%. Also, detection results for jujube (overall classification accuracy of 97.0%), and vegetable soybeans (95.6% overall classification accuracy) proved to be very high (Wu & Sun, 2013)

Also, optimal wavelengths in the range (400 - 1000 nm) has been used for predicting moisture content of banana by applying an exhaustive search with b-coefficients from PLSR models, resulted in coefficient of determination ( $r^2$ ) of 0.87.

Maturity stage of fruits, which is very important in determining the best harvest times, was the subject of study of hyperspectral imaging. Maturity evaluation required the definition of wavelength ratio and resulted in six optical indices (Ind1, Ind2, Ind3, IAD, rir, and Icarot,). These indices were calculated from data measured by multispectral imaging and spectrophotometer. Extracting mean reflectance spectra of grape seed in the range of 914–1715 nm to establish PLSR models showed an accurate prediction of maturation stage of grape seed with  $r^2$  being higher than 0.95 (Wu & Sun, 2013).

### **3.2.4 Hyperspectral Imaging for Assessing Quality and Safety of Meat**

According to Wang et al, meat was classified into three groups: fresh ( $\text{TVB-N} \leq 15 \text{ mg}/100 \text{ g}$ , pH 5.8–6.0), semi-fresh ( $\text{TVB-N} \leq 25 \text{ mg}/100 \text{ g}$ , pH 6.0–6.3), and spoiled ( $\text{TVB-N} > 25 \text{ mg}/100 \text{ g}$ , pH > 6.3) where TVB-N is meat freshness attribute and pH represent the meat's acidity. Meat samples were placed under halogen tungsten light source, and their hyperspectral images were acquired. Based on the reflectance spectra pretreated with Savitzky-Golay (SG) method at wavelengths of 635, 760, 575, and 980 nm, TVB-N was correctly predicted with  $R_p$

(coefficient of determination for prediction) of 0.90 and meat can be classified according to the previously mentioned groups with a total accuracy of 91% (Wang & Peng, 2018).

### **3.2.5 Meat Quality Evaluation by Hyperspectral Imaging Technique**

Elmasry et al, focused on studying beef meat tenderness, since tenderness is considered very important in the consumer perception of beef palatability. Different methods exist for the assessment of tenderness including the development of a pushbroom hyperspectral imaging system in the wavelengths range of 400-1000 nm with a lighting system to predict tenderness of 14 days aged cooked beef from hyperspectral images of fresh beef rib eye steaks. Slice shear force (SSF) values, a common traditional method that involves destructive measurement of beef tenderness by subjecting it to shear force, were considered as a tenderness reference and samples were divided in three different categories, namely tender ( $SSF \leq 205.80 \text{ N}$ ), intermediate ( $205.80 \text{ N} < SSF < 254.80 \text{ N}$ ), and tough ( $SSF \geq 254.80 \text{ N}$ ) (Elmasry, Barbin, Da-Wen, & Da-Wen, 2012).

The principal component analysis (PCA) was applied to a region-of-interest (ROI) of 200 × 600 pixels at the center of each steak. The three tenderness categories were predicted with an accuracy of 96.4%. Alternatively, the partial least squares regression (PLSR) was used, and the SSF value as a reference tenderness, the PLSR loading vectors were obtained. This model successfully classified 242 out of 314 samples with an accuracy of 77.0%.

This study considered another laboratory hyperspectral imaging system in the region of 400-1100 nm for assessing tenderness in 5-day aged beef. A multi-linear regression (MLR) approach was applied, and this technique identified the wavelength of 772 nm to be the most correlated with beef tenderness. Results concluded that hyperspectral images could predict tenderness with a high correlation coefficient ( $r$ ) of 0.94 and standard error of prediction (SEP) of 1.21 kg/cm<sup>2</sup> (Elmasry, Barbin, Da-Wen, & Da-Wen, 2012).

### **3.2.6 Evaluation of Near-Infrared Hyperspectral Imaging for Detection of Peanut and Walnut Powders in Whole Wheat Flour**

Due to the general utilization of processing equipment in, peanut and walnut can contaminate wheat flour, causing a major health risk to people that have allergy to nuts. For the avoidance of this problem, Zhao et al, studied the utilization of near-infrared hyperspectral

imaging in the inspection of peanut and walnut powder in whole wheat flour. The wavelengths in question is between 950 and 1700 nm. The partial least squares regression (PLSR) model was developed by adopting a combination of the standard normal variate and the Savitzky–Golay first derivative spectral transformation. In addition, a successive projection algorithm (SPA) and uninformative variable elimination (UVE) for feature wavelength selection were compared. The model yielded a determination coefficient of prediction ( $R_p^2$ ) of 0.987, and a root mean square error of prediction (RMSEP) of 0.373%. These results confirmed that the use of hyperspectral imaging in the detection of peanut and walnuts in whole wheat flour can be confidently in the production industries and can have a major health benefits to many allergic people (Zhao, Wang, Ni, & Chu, 2018).

### **3.3 Conclusion**

After careful study of the state of art regarding the use of hyperspectral imaging in the food industry, several studies were considered to be of great importance and have been briefly discussed in this chapter. These papers applied several models and algorithms such as linear discriminant analysis (LDA), quadratic discriminant analysis (QDA), stepwise discriminant analysis (SDA), partial least squares discriminant analyses (PLS-DA), successive projection algorithm (SPA), multi-linear regression (MLR), and the Savitzky-Golay (SG) method. The discussed studies computed several important factors which include coefficient of prediction ( $R_p^2$ ), correlation coefficient ( $r$ ), classification accuracy and overall accuracy. All these factors proved to be very high and almost all of them were above 0.9 or 90%. Also, several errors, including standard error of prediction (SEP) and root mean square error of prediction (RMSEP), were calculated and their results seemed to be relatively low.

Following these encouraging results, this research study tested the use of hyperspectral imaging on the monitoring of beef meat quality especially during several stages of deterioration. The research studied the reflectance of several signals and computed a cross-correlation matrix which related the time of deterioration to hyperspectral data.

# **CHAPTER 4: EXPERIMENTAL PROCEDURE & RESULTS**

## **4.1 Introduction**

This chapter presents the detailed experimental procedure that involves the measurement of hyperspectral data of red beef meat with respect to time. This is done to study the difference between the hyperspectral signature of fresh meat and that of deteriorating meat measured on an interval of 48 hours. After 48 hours, the meat would be clearly identified to be spoiled as its color and smell would be drastically changed and would be readily distinguished by the human senses. So there is no need to study it after the interval limit of 48 hours.

## **4.2 Hyperspectral Imaging Data Collection**

### **4.2.1 Material Selection & Sampling**

The food to be tested is the beef red meat. The ideal scenario is to measure the same piece of meat on a timeframe of 48 hours. However, the spectroradiometer used is the property of the National Council for Scientific Research (*CNRS*) and could only be used under the supervision of the center, which made the possibility of continuously using the device for 48 hours very difficult. Hence, a different approach was considered. The best alternative scenario was to take numerous samples of meat, remove each sample from the refrigerator at specific time, and then do all the measurements in a short space of time in the research center. 40 samples were taken from the same primal cut of filet beef meat weighing approximately 3 kilograms. The main piece of meat was trimmed and cleaned of all the white tissues and connecting fibers to ensure that all that remains is the red homogeneous meat. Also, since the spectroradiometer sensor measures a pixel which is equal to an area of 1 cm by 1 cm, the meat specimens were cut to a size that slightly exceeds this area. Also, the minimum thickness of meat was chosen to be 1 cm to ensure that adequate measurements were made.

The 40 samples of meat were divided in 13 batches, each is left at ambient temperatures for a different time. The time frames that were considered are 1 hour, 2 hours, 4 hours, 12 hours,

16 hours, 20 hours, 24 hours, 28 hours, 36 hours, 40 hours, 44 hours, 48 hours and finally fresh which is considered as 0 hours. Also, each sample was measured twice or thrice depending on the meat size resulting in a total of 94 signals. Each signal provided by the spectroradiometer is the average of 10 readings that the sensor automatically calculates. This results in a total of 940 readings.

#### **4.2.2 Meat Preparation**

The meat specimens were bought fresh from the butcher shop. They were then stored at a temperature of 4 degrees Celsius. The first 3 samples were removed from the refrigerator and placed at ambient temperature of 20 degrees 48 hours before the date of the measurement. Then, 4 hours later, another 3 samples of meat were removed and placed at ambient temperature. Again, after another 4 hours, 3 samples of meat were removed and placed at ambient temperature. This process was repeated every 4 hours, with exception of the times of 8 hours and 32 hours ignored for convenience reasons, until a total of 13 batches was at hand. Also, as the early hours of deterioration were considered important, there were 2 batches of meat removed at 1 hour and 2 hours before the measurement process. The preparation procedure was done at home and all the meat were transported by a mobile refrigerator that operates on the car's battery to ensure the desired storing temperature of fresh meat is maintained. Also, for the fresh batch, 4 samples were used.

To ensure orderliness and proper classification of meat batched, each batch was labeled, with each label referring to the time that each batch was removed from refrigeration and placed at ambient temperature. Also, to ensure that meat remain moist, plastic films were used to cover them. The figure below shows the arrangement of meat samples during the meat preparation phase.

Figure 21: The arrangement of meat samples during the meat preparation phase.



#### 4.2.3 Measurement Devices

To collect the reflectance spectra, a high-resolution spectroradiometer named **FieldSpec 4 Hi-Res** was used. This device is manufactured by ASD Inc. Company. It can detect the spectrum in the range between 350 and 2500 nm. The specifications of the spectroradiometer are given in the table below (ASD FieldSpec 4 Hi-Res: High Resolution Spectroradiometer, 2020).

The device is composed of numerous components:

- The main radiometer connected the probe via 1.5 m fiber connection wire.
- Power bank battery used to supply the radiometer.
- Specialized software installed on an auxiliary computer which is used for controlling the instrument and registering the data.
- White board used for calibration of the device before registration of the data.

There are other optional accessories. It should be noted that the connection between the computer and the spectrometer is wireless.

Table 1: FieldSpec 4 Hi-Res spectroradiometer specifications.

<b>Spectral Range</b>	350-2500 nm
<b>Spectral Resolution</b>	3 nm @ 700 nm 8 nm @ 1400/2100 nm
<b>Spectral sampling (bandwidth)</b>	1.4 nm @ 350-1000 nm 1.1 nm @ 1001-2500 nm
<b>Scanning Time</b>	100 milliseconds
<b>Stray light specification</b>	VNIR 0.02%, SWIR 1 & 2 0.01%
<b>Wavelength reproducibility</b>	0.1 nm
<b>Wavelength accuracy</b>	0.5 nm
<b>Maximum radiance</b>	VNIR 2X Solar, SWIR 10X Solar
<b>Channels</b>	2151
<b>Detectors</b>	VNIR detector (350-1000 nm): 512 element silicon array SWIR 1 detector (1001-1800 nm): Graded Index InGaAs Photodiode, Two Stage TE Cooled SWIR 2 detector (1801-2500 nm): Graded Index InGaAs Photodiode, Two Stage TE Cooled
<b>Input</b>	1.5 m fiber optic (25° field of view). Optional narrower field of view fiber optics available.
<b>Noise Equivalent Radiance (NEdL)</b>	VNIR 1.0 X10 <sup>-9</sup> W/cm <sup>2</sup> /nm/sr @700 nm SWIR 1 1.4 X10 <sup>-9</sup> W/cm <sup>2</sup> /nm/sr @ 1400 nm SWIR 2 2.2 X10 <sup>-9</sup> W/cm <sup>2</sup> /nm/sr @ 2100 nm
<b>Weight</b>	5.44 kg (12 lbs)
<b>Calibrations</b>	Wavelength, absolute reflectance, radiance*, irradiance*. All
<b>Computer</b>	Windows® 7 64-bit laptop (instrument controller)

Figure 22: FieldSpec 4 HI-RES spectroradiometer.



Crucial to the indoor measurement, an illuminator was used as a source of light named **ASD Illuminator Reflectance Lamp**. It provides light of different wavelengths in the range of 350 and 2500 nm having a constant intensity. The illuminator produces stable output with a smooth spectral curve into the SWIR range. The light lamp produces a specific beam maximizing the amount of light energy on the desired sample area while also minimizing stray light from the surrounding surfaces (ASD Illuminator Reflectance Lamp, 2020).

This Illuminator possesses several benefits as stated by the manufacturer, including:

- The 70-watt quartz-tungsten-halogen light source accompanied by an integrated reflector that provides stable illumination over the 350 to 2500 nm range.
- Stable output provides accurate and reliable reflectance measurements.
- Well-defined beam source maximizes light energy on specific sample area.
- Specific voltage regulation used for high stability light output.
- Several mount options for laboratory stands or tripods.

*Figure 23: ASD Illuminator Reflectance Lamp.*



These devices are the property of the Remote Sensing department of the **National Council for Scientific Research (CNRS)** in Lebanon who provided great assistance in the acquisition of the spectra of the meat samples.

#### **4.2.4 Hyperspectral Data Measurement**

After ensuring all the equipment and operating laptop have started up, the first step of the measurement process involves the calibration of the spectroradiometer sensor. This involves using a specific white plate that, theoretically, has a reflectance equal to 1. After calibration is done, each meat sample is placed under the illuminator that is placed on a tripod and situated at a distance of 20 cm. Sequentially, each of the 40 samples is placed under the sensor and its reflectance is measured. To ensure that accurate measurements are made, the sensor was held at a fixed position for all the samples. This guarantees that the difference in the reflectance of the different samples is not due to the sensor position (as the sensor is closer to the meat, higher light and thus higher reflectance is recorded) but rather due to the difference in the meat composition.

It should be noted that, every few measurements, the calibration is repeated as requested by the device. The spectroradiometer is connected wirelessly to a special laptop which contains the software designed to read and save the measured reflectance signals. The data is saved as (.asd) format which is then loaded into Matlab via a special toolbox called (matlab\_hyperspectral\_toolbox\_v0.07).

The data was saved according to a certain time nomination criterion. A signal  $Ah\_sxy$  specifies: the time that the meat is left in ambient temperature (A hour(s)), the sample number x along with the measurement number y of each sample. For example, the sample named 1h\_s12 refers to the second measurement of the first sample of the batch that is left at ambient temperature for 1 hour. Also, the sample named Fresh\_s41 refers to the first measurement of the fourth sample taken from the fresh batch.

Finally, all the measurements were conducted using the spectroradiometer within a short space of time approximated to be 15 minutes.

It should be mentioned that, the whole experiment was conducted two times. During the first experiment, a malfunction occurred to the illuminator and the measurement were conducted outdoor. This caused a significant amount of noise on certain bands (1355 – 1450 nm and 1800-1960 nm) that were related with water absorption. The noise was mainly due to fluctuation in the sun light.

Due to the unsatisfactory results, the decision was taken to repeat the experiment. Contributing to this decision was the fact that during the first experiment, the meat specimens were left exposed to the ambient air. This caused the meat to be dried (dehydrated) and became bacon-like. To prevent this, the meat was covered with plastic film and its thickness was increased. As can be seen by the results in the next section, the signals in the second experiment were noise free as the illuminator was repaired and properly used.

## 4.3 Results

### 4.3.1 Reflectance Graphs

As shown below, the reflectance of the different specimens within each batch were drawn with respect to a bandwidth range of 350 nm – 2400 nm.

*Figure 24: Reflectance of meat at time equal to 1 hour.*

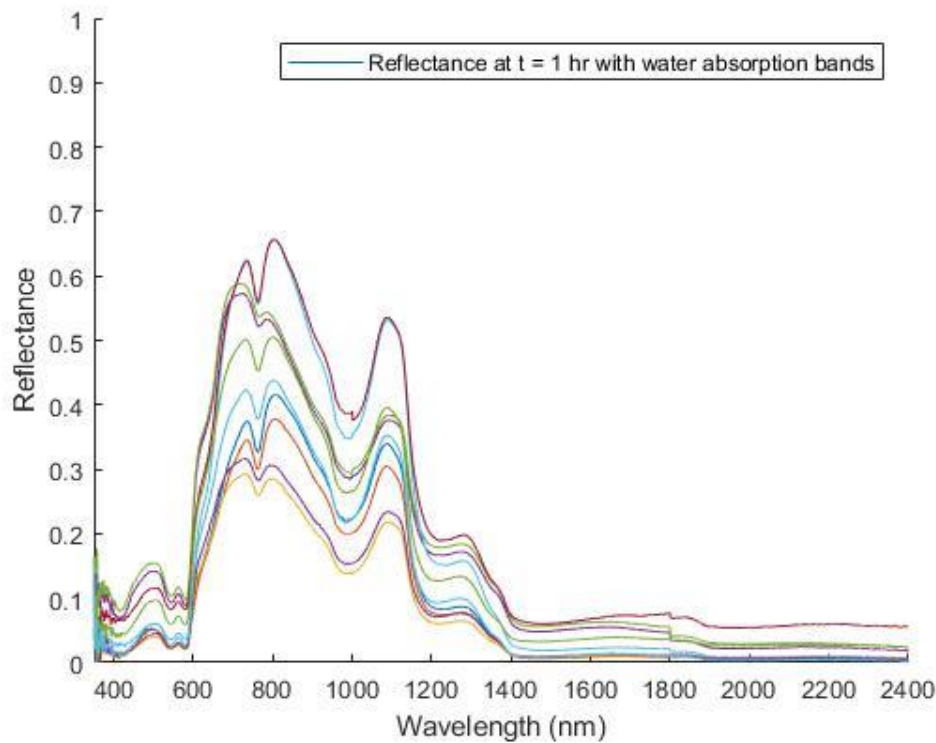


*Figure 25: Reflectance of meat at time equal to 2 hours.*

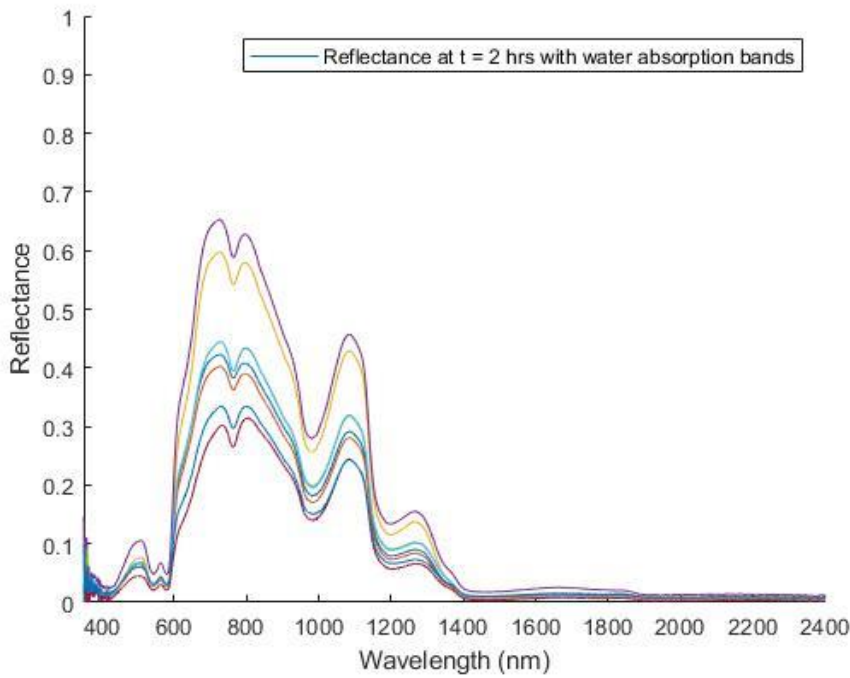


*Figure 26: Reflectance of meat at time equal to 4 hours.*

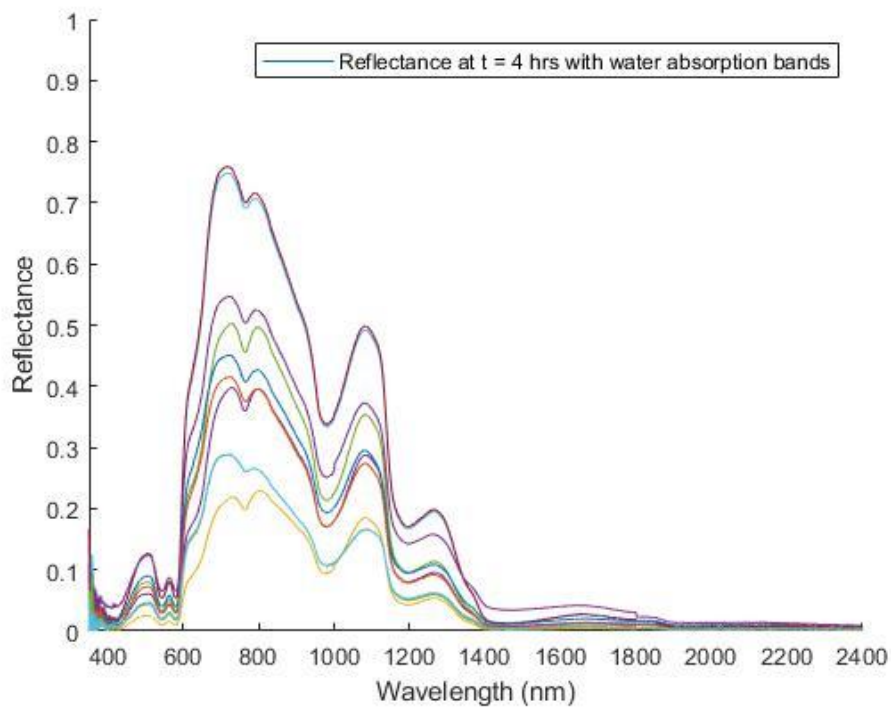


*Figure 27: Reflectance of meat at time equal to **12 hours**.*

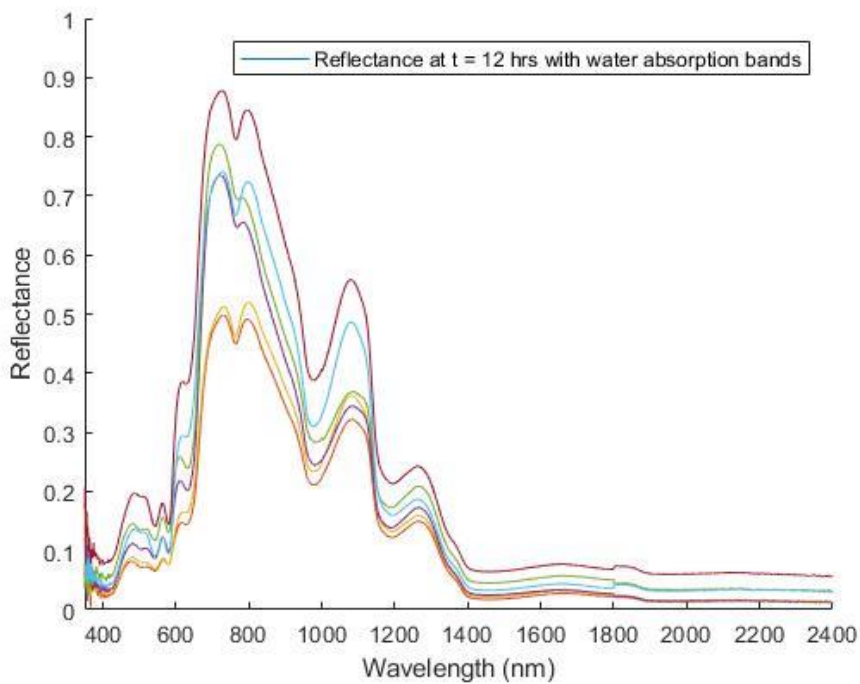


*Figure 28: Reflectance of meat at time equal to **16 hours**.*

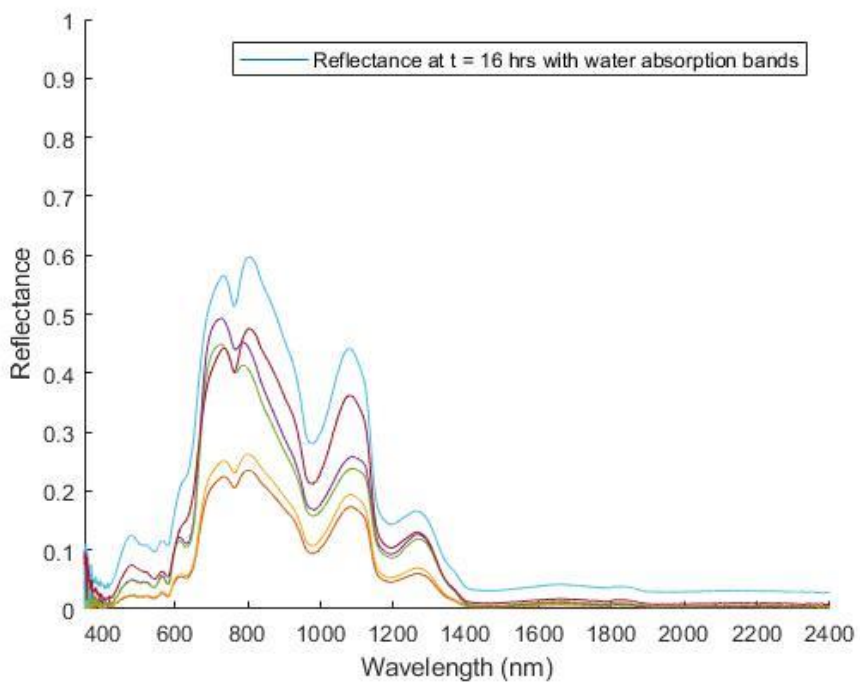


*Figure 29: Reflectance of meat at time equal to 20 hours.*

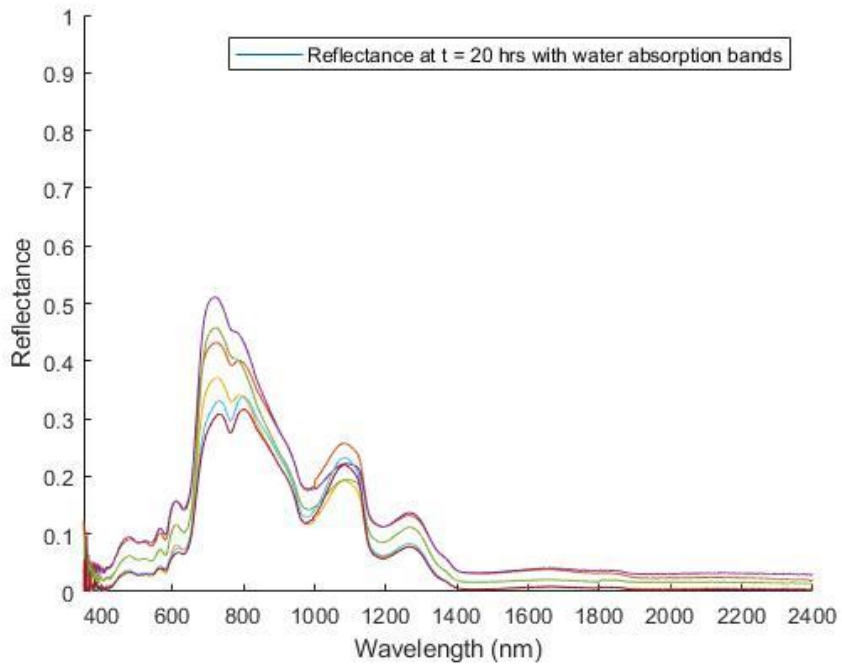


*Figure 30: Reflectance of meat at time equal to 24 hours.*

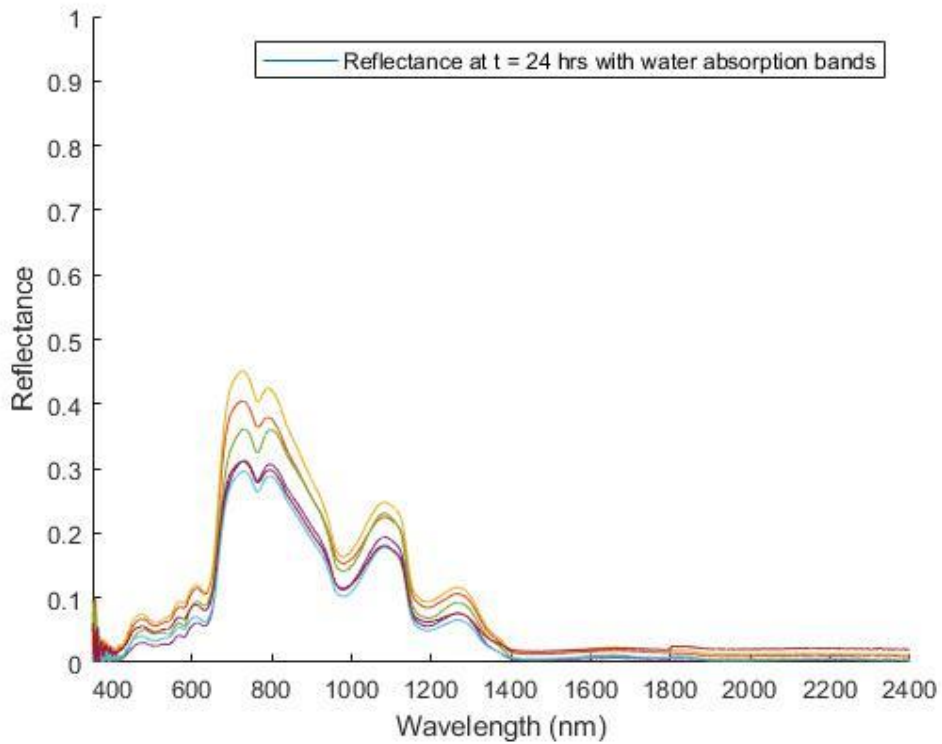


*Figure 31: Reflectance of meat at time equal to 28 hours.*

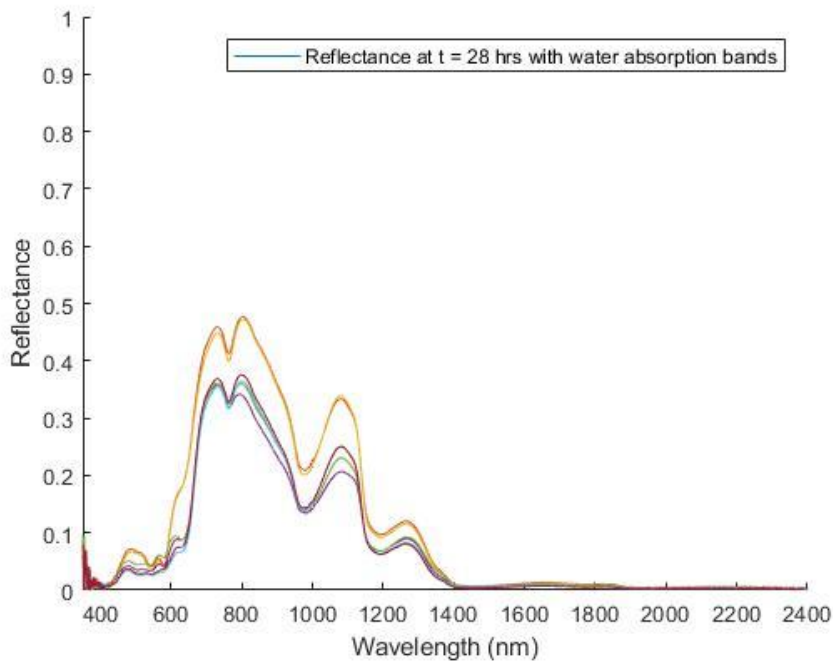


*Figure 32: Reflectance of meat at time equal to 36 hours.*

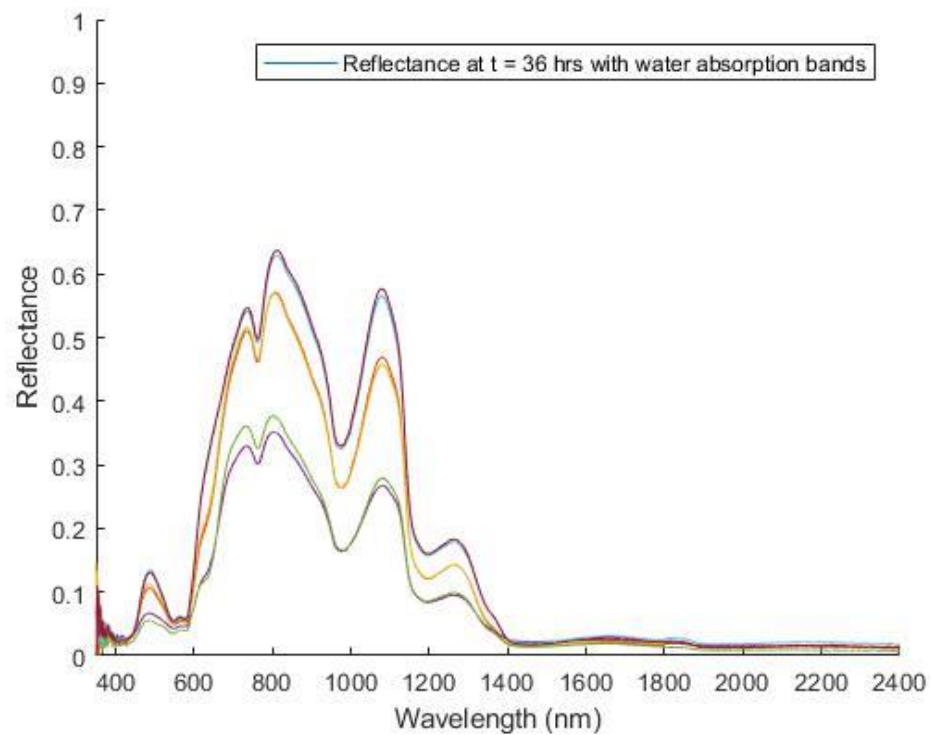


*Figure 33: Reflectance of meat at time equal to 40 hours.*

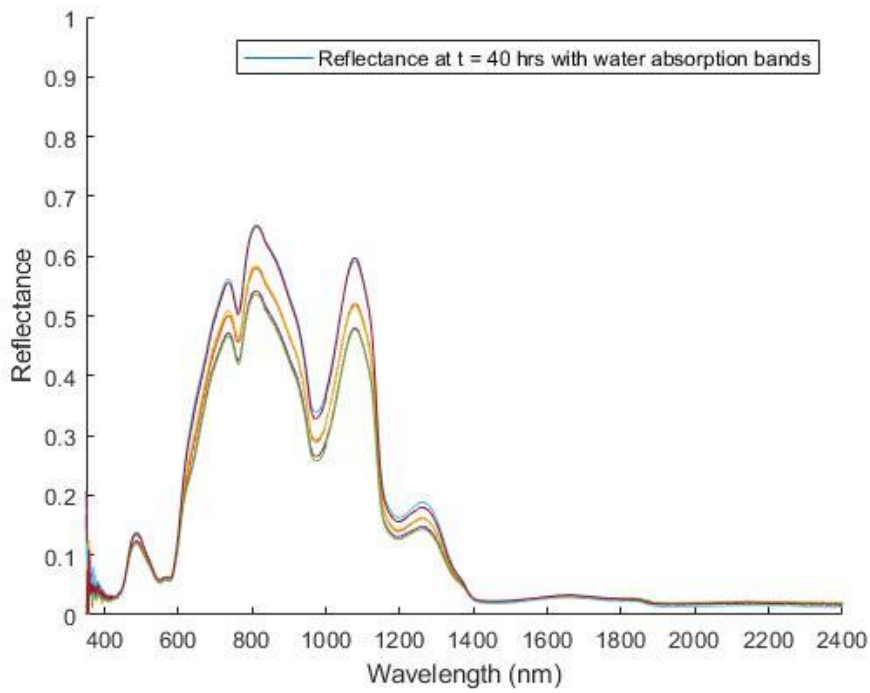


*Figure 34: Reflectance of meat at time equal to 44 hours.*

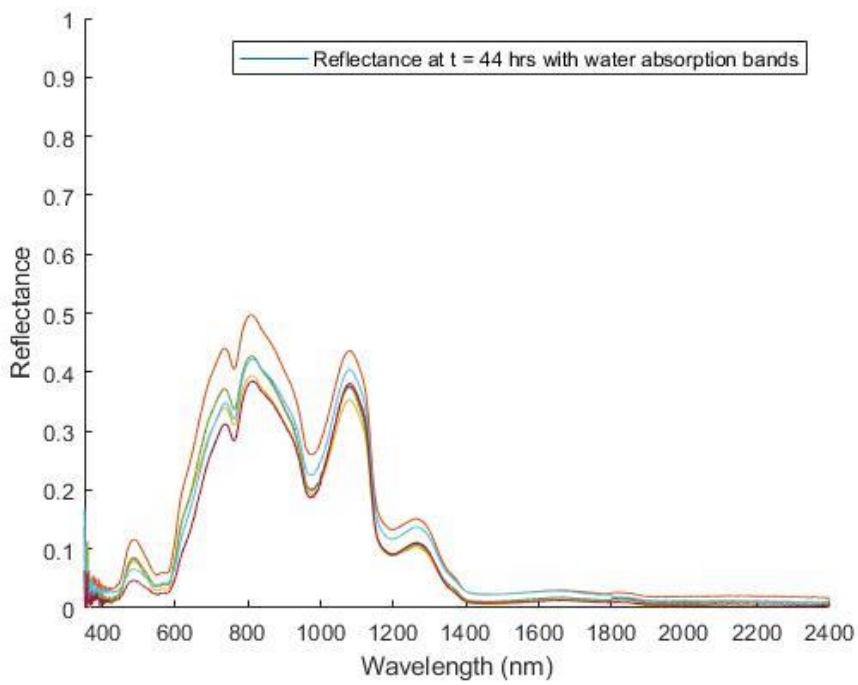


*Figure 35: Reflectance of meat at time equal to 48 hours.*

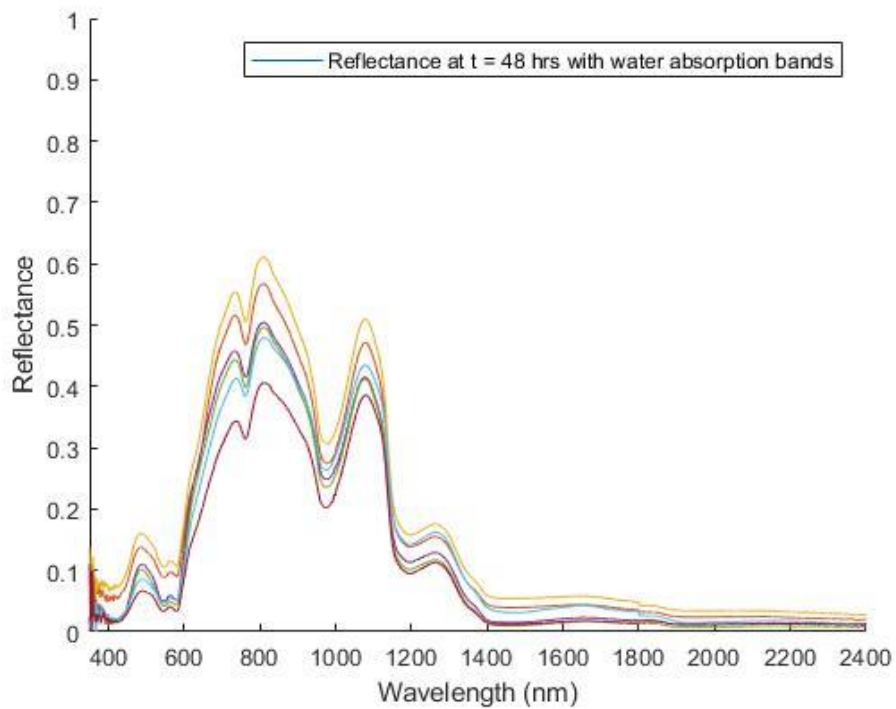
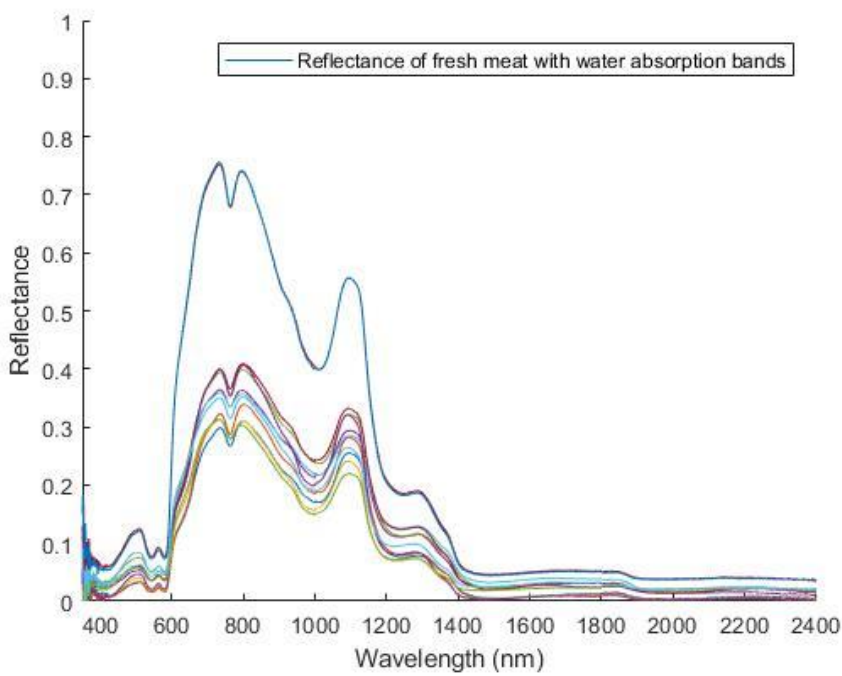


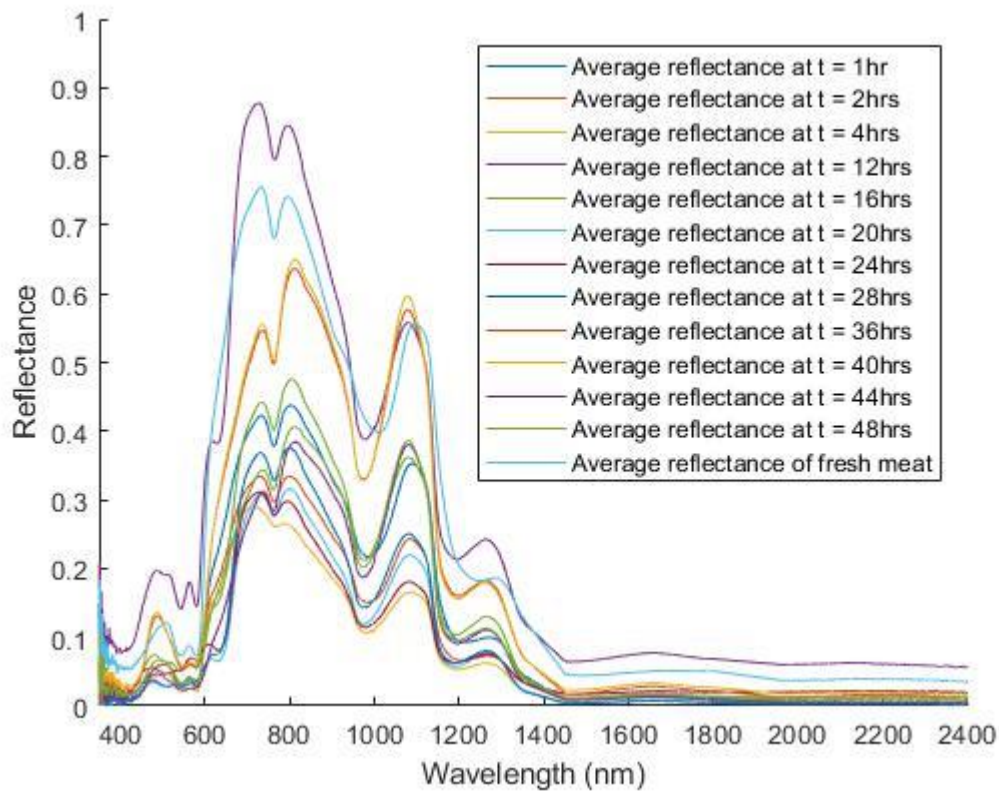
*Figure 36: Reflectance of fresh meat.*



As the results show, there is great discrepancies between the reflectance of the difference specimens within each given batch. Even though the meat were cut from the same main meat cut, and were removed at the same time from the refrigerator and placed at the same ambient temperature, and all the specimens appeared to be of similar color and at roughly the same deterioration phase, yet their respective reflectance differs.

In order to compare the different batches, the average of each batch was calculated, and then all the averages were drawn on the same graph as shown below.

*Figure 37: Reflectance of different meat batches.*



As can be seen from the graph, A clear correlation between the time of the batches and their respective reflectance cannot be established. The reflectance of meat batched do not increase or decrease as the time increases or decreases.

### **4.3.2 Cross-Correlations**

To better analyze the results, the difference between the peak of the fresh meat plot and all the other plots were calculated and the results were compiled in the below table.

*Table 2: The difference between the peaks of the different samples along with their respective bandwidth.*

	Difference Between Peaks	Bandwidth at this difference
Batch at t = 1 hour	0.33319	732
Batch at t = 2 hours	0.333	733
Batch at t = 4 hours	0.30428	797
Batch at t = 12 hours	0.32839	708
Batch at t = 16 hours	0.28658	656
Batch at t = 20 hours	0.29201	659
Batch at t = 24 hours	0.28849	657
Batch at t = 28 hours	0.2824	654
Batch at t = 36 hours	0.31713	679
Batch at t = 40 hours	0.31642	678
Batch at t = 44 hours	0.32504	691
Batch at t = 48 hours	0.32768	703

As the table shows, the difference between the peaks of the graphs fluctuates. As the time of the batches increase, the difference between the peaks do not increase or decrease. Therefore, a correlation could not be established.

To further analyze the results, the cross-correlation between the different signals have been calculated using the correlation matrix which is calculated using the Matlab command ‘corrcoef’ as follows: “Correlation\_matrix = corrcoef(matrix’);” the matrix titled ‘matrix’ is composed of all the averages vectors that have been previously calculated.

The below table shows the normalized cross-correlation matrix, which is a 13x13 matrix, showing the correlation between each of the 13 averages of the different samples. As you can see, the matrix is symmetric, whose diagonal vector values are all equal to 1, as it relates each signal to itself. Furthermore, the values in the matrix did not show differences between the samples named fresh and other samples taken at different times as they all ranged from 0.95 to 0.99. In other words, meat taken at time equal to 48 hours (0.99551) was not significantly different than that taken at time equal 1 hour (0.996017) when their correlation with the fresh sample was computed. This would reinforce earlier results that all meat samples are similarly related regardless of their deterioration level or bacteria content.

Table 3: Cross-Correlation table showing the correlation between the averages of the different samples.

	Fresh	t = 1 hr	t = 2 hrs	t = 4 hrs	t = 12 hrs	t = 16 hrs	t = 20 hrs	t = 24 hrs	t = 28 hrs	t = 36 hrs	t = 40 hrs	t = 44 hrs	t = 48 hrs
Fresh	1 7	0.99601 7	0.9811 8	0.98746 6	0.99218 9	0.98189 3	0.97070 7	0.98211 7	0.98935 6	0.98867 3	0.97185 4	0.98573 2	0.99551 4
t = 1 hr	0.99601 7	1 8	0.99271 3	0.99492 4	0.98757 9	0.98083 2	0.97957 9	0.98261 6	0.97762 3	0.97737 6	0.95301 3	0.97234 5	0.99473 4
t = 2 hrs	0.9811 8	0.99271 1	0.99295 7	0.96821 9	0.96667 9	0.97771 6	0.96922 2	0.95000 8	0.94952 5	0.91604 3	0.94153 9	0.98798 9	
t = 4 hrs	0.98746 6	0.99492 3	0.99295 7	1 3	0.98668 2	0.98662 9	0.99199 9	0.98845 6	0.96609 4	0.96551 2	0.94047 2	0.95974 6	0.98728 4
t = 12 hrs	0.99218 9	0.98757 4	0.96821 9	0.98668 3	1 8	0.99475 4	0.98104 5	0.99372 2	0.99077 4	0.99059 7	0.98128 5	0.98935 1	0.98070 1
t = 16 hrs	0.98189 3	0.98083 9	0.96667 2	0.98662 8	0.99475 1	0.99149 1	0.99853 1	0.97504 2	0.97546 1	0.96724 1	0.97410 7	0.97122 3	
t = 20 hrs	0.97070 7	0.97957 2	0.97771 6	0.99199 9	0.98104 4	0.99149 1	0.99280 2	0.94927 6	0.94967 3	0.93125 4	0.94580 2	0.96727 6	
t = 24 hrs	0.98211 7	0.98261 2	0.96922 6	0.98845 5	0.99372 1	0.99853 2	0.99280 1	0.97236 8	0.97279 3	0.96292 8	0.97133 7	0.97245 4	
t = 28 hrs	0.98935 6	0.97762 6	0.95000 8	0.96609 4	0.99077 2	0.97504 2	0.94927 6	0.97236 8	1 8	0.99960 8	0.99275 6	0.99836 3	0.97477 3
t = 36 hrs	0.98867 3	0.97737 3	0.94952 5	0.96551 2	0.99059 4	0.97546 1	0.94967 3	0.97279 3	0.99960 8	1 7	0.99336 4	0.99879 6	0.97306 6
t = 40 hrs	0.97185 4	0.95301 6	0.91604 3	0.94047 7	0.98128 1	0.96724 1	0.93125 4	0.96292 8	0.99275 6	0.99336 7	1 4	0.99637 2	0.94920 2
t = 44 hrs	0.98573 2	0.97234 5	0.94153 9	0.95974 6	0.98935 5	0.97410 7	0.94580 2	0.97133 7	0.99836 3	0.99879 4	0.99637 4	1 1	0.96788 1
t = 48 hrs	0.99551 4	0.99473 4	0.98798 9	0.98728 4	0.98070 1	0.97122 3	0.96727 6	0.97245 4	0.97477 3	0.97306 6	0.94920 2	0.96788 2	1 1

## **4.4 Conclusion**

As a conclusion, the results showed a lack of a correlation between the signals that have been taken from different samples referring to meat that are in different stages of deterioration. This was visible by calculating the difference in peaks of the different plots as well as from the correlation matrix that was computed on Matlab.

## CHAPTER 5: CONCLUSION

Hyperspectral imaging is a very important field of study. Its applications are virtually limitless, and they include various fields that encompass food, agriculture, biology lab, pharmaceuticals, environmental monitoring, surveillance, astronomy among others. This thesis tackled the application of hyperspectral imaging in food monitoring, more specifically studying the relationship between meat degradation and their hyperspectral data signatures.

During this research, 96 hyperspectral signals were analyzed. Their reflectance on a wavelength range of 350-2400 nm was studied and drawn on several graphs showing the plots of meat signals that have been left out at ambient temperature for 13 time periods. It was seen from the graphs that meat samples from the same batch, that had similar qualities and were at the same deterioration level, had fairly different light signatures. This may be attributed to macroscopic differences in meat samples at the molecular level. Even though were taken from the same beef cut, and appeared to be homogeneous and similar in color, their signatures showed some differences.

In order to study the relation between deterioration level and hyperspectral data for all the different meat samples and batches, the normalized cross-correlation was computed, with values normally ranging from 0 to 1. The normalized cross-correlation showed the correlation between the fresh meat samples and all the other batches of meat that have different time stamps. Also, it studied the correlation of each batch with all the other batches. This resulted in a 13x13 matrix whose values were very similar and ranged from 0.95 to 0.99. These results implied that this research could not relate deterioration level to hyperspectral data of meat. This conclusion was further enforced from the graph showing the plots of each batch signature that had different deterioration levels. Also, by computing the difference between the peaks of each plot and comparing their values, the degradation level of meat could not be determined. This failure to predict meat degradation level based on their hyperspectral level could be attributed to many factors, they include:

- Noise and fluctuation in the ambient atmosphere. Even some types of noise were filtered, others could have affected the readings.
- Instrument errors and variations that could have existed in the spectroradiometer, illuminator or any part of the sensing system.
- Hyperspectral measurement variation that may have resulted from the distance between the meat and spectroradiometer sensor. Even though special attention was placed on locating the sensor at equal distance for all the samples, the human hand holding could have possibly moved, resulting in measurement variations.
- Macroscopic variation in the meat composition. Although all the meat samples appeared to be very similar, there may have existed variations in their composition that may be due to some unseen fat tissue or tendons under the surface.

It should be noted that this study has an added complexity due to the study of a relatively high number of deterioration levels. A “good or bad meat” scenario could have been easier to analyze by studying two classes the first one being a fresh meat and the second being a spoiled one. Instead of considering 13 different batches, a relatively smaller number could have been less complex.

In a future work, the identification of foreign materials in ground meat could be studied. Since different materials have different spectral characteristics, hyperspectral imaging should be able to identify the existence of materials such as metal or plastic that may have combined with meat during the grounding process.

## REFERENCES

- Advanced applications of hyperspectral imaging technology for food quality and safety analysis and assessment. (2013).
- ASD FieldSpec 4 Hi-Res: High Resolution Spectroradiometer.* (2020). Retrieved from Malvern Panalytical: <https://www.malvernpanalytical.com/en/products/product-range/asd-range/fieldspec-range/fieldspec4-hi-res-high-resolution-spectroradiometer>
- ASD Illuminator Reflectance Lamp.* (2020). Retrieved from AZO Materials: <https://www.azom.com/equipment-details.aspx?EquipID=5409>
- Augustyn, A., Bauer, P., & Duignan, B. (2018). *Electromagnetic spectrum*. Retrieved from Britannica Encyclopedia: <https://www.britannica.com/science/electromagnetic-spectrum>
- Bit Depth.* (2019). Retrieved from Cambridge In Color: <https://www.cambridgeincolour.com/tutorials/bit-depth.htm>
- Bossoon, P. (2015). *Hyperspectral Imaging Technology in Food and Agriculture*. New York: Springer.
- Campbell, A. (2000). *The Designer's Lexicon*. San Francisco: Chronicles Books.
- Chamberland, M., Farley, V., Vallières, A., & Belhum, L. (2005). *"High-Performance Field-Portable Imaging Radiometric Spectrometer Technology For Hyperspectral imaging Applications*.
- Chang, C.-I. (2003). *Hyperspectral Imaging: Techniques for Spectral Detection and Classification*. Springer Science & Business Media.
- Davies, O. L. (2015, December 3). *WHO's first ever global estimates of foodborne diseases find children under 5 account for almost one third of deaths*. Retrieved from World Health Organization: <https://www.who.int/news-room/detail/03-12-2015-who-s-first-ever-global-estimates-of-foodborne-diseases-find-children-under-5-account-for-almost-one-third-of-deaths>
- Detect Food Spoilage with Sensors.* (2017, November 5). Retrieved from ElectronicsForu: <https://www.electronicsforu.com/technology-trends/detect-food-spoilage-sensors>

*Digital Images*. (2020, March 05). Retrieved from Encyclopedia:

<https://www.encyclopedia.com/computing/news-wires-white-papers-and-books/digital-images>

Elmasry, G., Barbin, D. F., Da-Wen, S., & Da-Wen, P. (2012). Meat Quality Evaluation by Hyperspectral Imaging Technique: An Overview. *Critical Reviews in Food Science and Nutrition*, 689-711.

ElMasry, G., Wang , N., ElSayed, A., & Ngadi, M. (2006). 3.2.1 Hyperspectral Imaging for nondestructive determination of some quality attributes for strawberry. *Science Direct*.

Fletcher, B., & Mullane, K. (2018). Advances in meat spoilage detection: A short focus on rapid methods and technologies. *Journal of Food*.

*Food safety*. (2019, June 4). Retrieved from World Health Organization:  
<https://www.who.int/news-room/fact-sheets/detail/food-safety>

Gibbons, K. P. (2014, MARCH 1). *Hyperspectral Imaging What is it? How does it work?* Retrieved from Tech Briefs:  
<https://www.techbriefs.com/component/content/article/tb/supplements/ptb/features/applications/19507>

Gonzalez, R. (2018). *Digital image processing*. New York: Pearson.

Hirsch, R. (2004). *Exploring Colour Photography: A Complete Guide*. Laurence King Publishing.

Huang, H., Liu, L., & Ngadi, M. O. (2014). Recent Developments in Hyperspectral Imaging for Assessment of Food Quality and Safety. *Multidisciplinary Digital Publishing Institute (MDPI)*, 7249-7250.

*Hyperspectral Imaging Applications*. (2019). Retrieved from Delta optical thin film:  
<https://www.deltaopticalthinfilm.com/hyperspectral-imaging-applications/>

*Important Applications of Hyperspectral Image*. (2016, February 6). Retrieved from Grindgis:  
<https://grindgis.com/remote-sensing/10-important-applications-of-hyperspectral-image>

Johnson, S. (2006). *Stephen Johnson on Digital Photography*. O'Reilly.

- Mustafa, F., & Andreeșcu, S. (2018). Chemical and Biological Sensors for Food-Quality Monitoring and Smart Packaging. *Multidisciplinary Digital Publishing Institute (MDPI)*, 4-7.
- Qin, J., Moon, K. S., & Chao, K. (26 January 2017). Line-Scan Hyperspectral Imaging Techniques for Food Safety and Quality Applications. *MDPI*.
- RGB*. (2019, May 17). Retrieved from Tech terms: <https://techterms.com/definition/rgb>
- RGB vs CMYK*. (2019, June). Retrieved from 99 Designs: <https://99designs.com/blog/tips/correct-file-formats-rgb-and-cmyk/>
- Sullivan, G., Ohm, J.-R., & Wiegand, T. (2013). Overview of the High Efficiency Video Coding (HEVC) Standard. *IEEE Transactions on Circuits and Systems for Video Technology*.
- The Electromagnetic Spectrum*. (2013, March). Retrieved from NASA Goddard Space Flight Center: <https://imagine.gsfc.nasa.gov/science/toolbox/emspectrum1.html>
- Wang, W., & Peng, Y. (2018). *Hyperspectral Imaging in Agriculture, Food and Environment*. IntechOpen.
- What is bit depth?* (2018). Retrieved from Educational Technology Clearinghouse: <https://etc.usf.edu/techease/win/images/what-is-bit-depth/>
- Wu, D., & Sun, D.-W. (2013). Advanced applications of hyperspectral imaging technology for food quality and safety analysis and assessment. *Elsevier*.
- Zhao, X., Wang , W., Ni, X., & Chu, X. (2018). Evaluation of Near-Infrared Hyperspectral Imaging for Detection of Peanut and Walnut Powders in Whole Wheat Flour. *MDPI*.